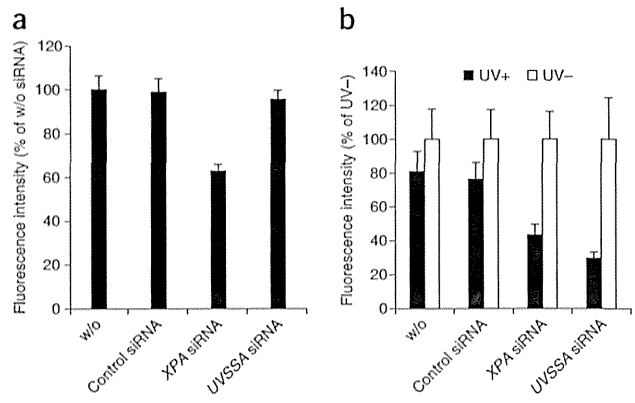

Figure 8 | RNA interference experiments for UDS and RRS assay. 48BR cells were seeded on a plastic 96-well plate and transfected with siRNA designed for *XPA*, *UVSSA* or nontargeting control. (**a**) UDS assay: at 72 h after siRNA transfection, cells were UV irradiated (20 J/m^2 UVC irradiation), followed by EdU incorporation and detection as described in the main PROCEDURE (Steps 6–16). (**b**) RRS assay: at 72 h after siRNA transfection, cells were UV irradiated (black bars, 9 J/m^2 UVC irradiation; white bars, no UV irradiation), followed by 4 h of incubation with DMEM supplemented with 1% (vol/vol) FBS. EU incorporation and detection were performed as described in the main PROCEDURE (Steps 6–16). Bars and error bars represent average fluorescence intensity (in arbitrary units) of quadruplicates and s.d., respectively. UDS was normalized to activity measurement in mock transfection control cells. RRS was normalized to activity measurement in nonirradiated cells. w/o, without siRNA transfection.

captured field are evaluated and the average fluorescence intensity of 25 different fields is calculated for each well (**Supplementary Notes 1** and **2**).

Cell sensitivity assay after UV irradiation. The method is summarized in **Box 1** and **Figure 5a**. Normal control and UV-sensitive patient–derived fibroblasts are seeded in duplicate on a plastic 96-well plate and cultured in FBS-supplemented DMEM (**Fig. 3d**). Cells are irradiated with different doses of UVC, followed by incubation in FBS-supplemented DMEM. The steps of EdU incorporation, cell fixation, azide-coupling reaction and DAPI staining are the same as those described in the UDS assay. Image acquisition and data processing are automated using the VTI system as described above. All cells in a single captured field are evaluated and the average fluorescence intensity of 50 different fields is calculated for each well (**Supplementary Note 3**).

Virus complementation assay. The lentivirus complementation assay (summarized in **Box 2** and **Fig. 5b**) can be used to determine complementation groups. Cells are seeded on a 96-well plate (**Fig. 3b–d**), precultured for 16 h and infected with lentivirus carrying DNA repair–related genes, followed by 48–72 h of incubation to allow for protein expression. UDS, RRS and/or cell sensitivity assays are then carried out as described above. Viral infection efficiencies are determined by immunofluorescence staining of the V5-tagged proteins, which involves seeding cells on a glass-bottomed 96-well plate (**Fig. 3e**) rather than a plastic plate. At 72 h after infection with the lentiviruses, cells are fixed and permeabilized, followed by blocking and incubation with anti-V5 antibody. After washing with PBST (PBS with Tween 20), cells are incubated with Alexa Fluor 488–conjugated secondary antibody. Image acquisition and data processing are automated using the VTI system. The average fluorescence intensity of ten different fields is evaluated and infection efficiency is calculated. A conventional electroporation method can be used as an alternative to lentivirus-based gene transduction (**Supplementary Method 5** and **Supplementary Fig. 4**).

RNA interference assay. siRNA oligos designed for the *XPA* or *UVSSA* genes and for a nontargeting control were purchased from Nippon EGT, Dharmacon or Sigma-Aldrich. A mixture of three different double-stranded siRNA oligonucleotides designed for different places of target gene was used for transfection. siRNA transfection was performed using the X-tremeGENE transfection reagent (Roche) according to the manufacturer's instructions. Experimental procedures are summarized in **Box 3** and **Figures 3f** and **5c**. At 72 h after siRNA (10 nM) transfection, UDS and RRS assays were carried out as described in the sections above.

MATERIALS

REAGENTS

- *Primary fibroblast cells established from patients and normal individuals:* normal 48BR (ref. 36), XP patient–derived XP15BR (XPA)[37], XP21BR (XPC)[32], CS patient–derived CS2AW (CSA)[38], XP-CS-Fanconi anemia complex patient–derived XPCS1CD (XPF/CS/FA)[34], XP-CS complex patient–derived CS1USAU (XPF/CS)[34], UVSS patient–derived Kps3 (UVSSA)[15] and severe combined immunodeficiency (SCID) patient–derived NM-720 (ref. 35) cells were used here ▲ **CRITICAL** The use of human tissues should adhere to all relevant ethics protocols and regulations. Informed consent should be obtained for the use of all patient samples.
- DMSO (Sigma, cat. no. D5879)
- D-PBS (Wako, cat. no. 045-29795)
- Trypsin-EDTA, 0.05% (wt/vol) (Gibco, cat. no. 25300-062)
- DMEM (Wako, cat. no. 043-30085)
- FBS (Gibco, cat. no. 26140-079)
- Penicillin-streptomycin, 100× (Wako, cat. no. 168-23191)
- Hexadimethrine bromide (Polybrene; Sigma, cat. no. H9268)
- 5-Ethynyl-2′deoxyuridine (EdU; Invitrogen, cat. no. A10044)
- 5-Ethynyluridine (EU; Invitrogen, cat. no. E10345)
- Sucrose (Wako, cat. no. 196-00015)
- Formaldehyde solution, 37% (vol/vol) (37% formalin; Wako, cat. no. 064-00406) ! **CAUTION** Formaldehyde solution is toxic; it should be used in a hood and handled with gloves.
- Triton X-100 (Wako, cat. no. 169-21105)
- Tween 20 (Wako, cat. no. 166-21115)
- 2-Amino-2-hydroxymethyl-1,3-propanediol (Tris base; Wako, cat. no. 015-20093)
- Hydrochloric acid, 20% (vol/vol) (HCl; Wako, cat. no. 083-03435)
- Copper (II) sulfate ($CuSO_4$; Wako, cat. no. 032-12511)
- Sodium ascorbate (Wako, cat. no. 198-01251)
- Alexa Fluor 488–azide (Invitrogen, cat. no. A10266)
- Alexa Fluor 488–conjugated goat anti-mouse IgG (H+L) antibody (Invitrogen, cat. no. A11029)
- DAPI solution (Dojindo, cat. no. D523-10)
- Anti-V5-tag mouse monoclonal antibody (MBL, cat. no. M167-3)
- X-tremeGENE siRNA transfection regent (Roche, cat. no. 04476093001)
- pLenti6.3/V5-TOPO and pLenti6.3/V5-TOPO TA cloning kits (Invitrogen, cat. no. K5315-20)
- ViraPower packaging mix (Invitrogen, cat. no. K4975-00)
- Lipofectamine 2000 (Invitrogen, cat. no. 11668019)

- PEG-it virus precipitation solution (System Biosciences, cat. no. LV810A)
- siRNA oligonucleotides: siXPA-1 (5′-CACCUCUUAAAUUUAUUGUTT-3′, Sigma-Aldrich, cat. no. NM_000380); siXPA-2 (5′-CUACUGGAGGCAU GGCUAATT-3′; Sigma-Aldrich, cat. no. NM_000380); siXPA-3 (5′-CUUU GAUUUGCCAACUUGUTT-3′; Sigma-Aldrich, cat. no. NM_000380); siUVSSA-1 (NIPPON EGT, cat. no. NRU029868); siUVSSA-2 (NIPPON EGT, cat. no. NRU029867); siUVSSA-3 (NIPPON EGT, cat. no. NRU029866); ON-TARGETplus siRNA control (Dharmacon, cat. no. D-001810-10)

EQUIPMENT

- Tissue culture flask of 75 cm^2 (BD Falcon, cat. no. 353136)
- Microtest 96-well plate, flat bottom (BD Falcon, cat. no. 353072)
- Microwell 96-well optical-bottom plates with coverglass base, black (Nunc, cat. no. 164588)
- Water bath (Taitec, SDmini, cat. no. 0034942-000)
- CO_2 incubator (Astec, SCA-165DS)
- Bio-clean bench (Panasonic, MCV-B131F)
- Test-tube mixer (Taitec, Se-08, cat. no. 0061271-000)
- Capsulefuge (Tomy, cat. no. PMC-060)
- Bright-field microscope (Leica DM IL LED inverted microscope)
- Counting chambers (Hirschmann, cat. no. 8100104)
- Rotator (Taitec, RT-50)
- Tabletop centrifuge (Kubota, 2420)
- Refrigerator/freezer (Panasonic, MPR-414F; MPR-U339)
- Cellomics ARRAY^{SCAN} VTI HCS system (Thermo Scientific)
- Fluorescence microscope (Carl Zeiss, Axio Observer Z1)
- UV cross-linker (UVP, CL-1000)
- UVX radiometer (UVP, 97-0015-02)
- pH meter (Horiba, F-52)
- Electronic scales (Shinko, AJ2-320)
- Aspirator (Biosan, FTA-1)
- Reagent reservoirs, 25 ml, disposable (INA-OPTIKA, cat. no. 4312 and AS ONE, cat. no. 2-7844-02)
- Pipette aid (Gilson, macroman)
- Multichannel pipette (Thermo Scientific, Finnpipette F2 8-channel 30–300 µl)
- Pipetman (Gilson)
- Tips (FastGene, 0.1–10 µl, cat. no. 23571T; 1–200 µl, cat. no. 15281T and 100–1,000 µl, cat. no. 10231T)
- Tubes (BD Falcon, 50 ml, cat. no. REF352070 and 15 ml, cat. no. REF352096)

REAGENT SETUP

EdU Dissolve 50 mg of EdU in 19.8 ml of 100% DMSO to a final concentration of 10 mM. Divide the solution into 100-µl aliquots and store them at −20 °C for 1–2 years.

EU Dissolve 5 mg of EU in 93.2 µl of 100% DMSO to a final concentration of 200 mM. Store the solution at −20 °C for up to 1 year.

$CuSO_4$ Dissolve 1.25 g of $CuSO_4$-$5H_2O$ in 50 ml of H_2O to a final concentration of 100 mM. Store the solution at 4 °C for up to 6 months.

Sodium ascorbate Dissolve 0.1 g of sodium ascorbate in 450 µl of H_2O to a final concentration of 1 M. The solution must be freshly prepared each time.

Alexa Fluor 488-azide Dissolve 0.5 mg of Alexa Fluor 488–azide in 140 µl of 100% DMSO to a final concentration of 4.15 mM. Shield it from light and store it at −20 °C for up to 6 months.

1 M Tris-HCl buffer, pH 7.3 Combine 12.41g of Tris base in 100 ml of H_2O, and add 6 N HCl until the pH stabilizes at 7.3. Store the buffer at room temperature (25 °C) for up to 3 months.

Fix buffer A Prepare 300 mM sucrose, 2% (vol/vol) formaldehyde and 0.5% (vol/vol) Triton X-100 in PBS. For 10 ml, combine 1.03 g of sucrose, 0.5 ml of 37% (vol/vol) formalin and 50 µl of 100% Triton X-100, and bring the volume to 10 ml with PBS. ▲ **CRITICAL** This solution has a short shelf life. It should be freshly prepared each time to avoid insufficient permeabilization.

Fix buffer B Prepare 3.7% (vol/vol) formaldehyde in PBS by adding 1 ml of 37% (vol/vol) formalin to 9 ml of PBS. ▲ **CRITICAL** This solution has a short shelf-life. It should be freshly prepared each time to avoid insufficient fixation and fluorescence fading.

Fix buffer C Prepare 300 mM sucrose, 2% (vol/vol) formaldehyde and 0.2% (vol/vol) Triton X-100 in PBS. For 10 ml, combine 1.03 g of sucrose, 0.5 ml of 37% (vol/vol) formalin and 20 µl of 100% Triton X-100, and make up the volume to 10 ml with PBS. ▲ **CRITICAL** This solution has a short shelf life. It should be freshly prepared each time to avoid insufficient permeabilization.

Azide-coupling solution Prepare 10 µM Alexa Fluor 488–azide in 50 mM Tris-HCl (pH 7.3), supplemented with 4 mM $CuSO_4$ and 10 mM sodium ascorbate. Combine 180.5 µl of H_2O with 9.5 µl of 1 M Tris-HCl buffer, 8 µl of 100 mM $CuSO_4$, 2 µl of 1 M sodium ascorbate and 0.5 µl of 4.15 mM Alexa Fluor 488–azide (in total 200.5 µl, sufficient for five wells). ▲ **CRITICAL** Add sodium ascorbate and Alexa Fluor 488–azide at the end (immediately before staining), and mix carefully to avoid precipitation. Freshly prepare the solution each time, as fluorescence fades quickly.

PBST Add 250 µl of 100% Tween 20 to 500 ml of PBS to obtain a final concentration of 0.05% (vol/vol) Tween 20 in PBS. Store the solution at room temperature for up to 6 months.

Cell strains and cultures Unless otherwise stated, all cell strains used in the development and testing of this protocol were primary fibroblasts derived from patients who were clinically diagnosed with XP, CS (including XP/CS and XP/CS-Fanconi complexes) or SCID, or cells from a healthy donor. Normal 48BR (ref. 36), XP patient–derived XP15BR (XPA)[37], XP21BR (XPC)[32], CS patient–derived CS2AW (CSA)[38], XP-CS-Fanconi complex patient–derived XPCS1CD (XPF/CS/FA)[34], XP-CS complex patient–derived CS1USAU (XPF/CS)[34], UV^{S}S patient–derived Kps3 (UVSSA)[15] and SCID patient–derived NM-720 (ref. 35) cells were used. All cells were cultured in 75-cm^2 flasks and maintained in DMEM supplemented with 10% (vol/vol) FBS and 1× penicillin-streptomycin. ▲ **CRITICAL** The use of human tissues should adhere to all relevant ethics protocols and regulations. Informed consent should be obtained for the use of all patient samples.

Lentivirus Recombinant lentivirus particles expressing DNA repair genes were produced using the ViraPower lentiviral expression system according to the manufacturer's instructions (Invitrogen, pLenti6.3/V5-TOPO and pLenti7.3/V5-TOPO TA cloning kits: http://tools.lifetechnologies.com/content/sfs/manuals/plenti6_3_7_3_v5_topo_ta_man.pdf). Briefly, full-length human *XPA*, *XPC*, *XPF* and *CSA* cDNAs were amplified from a first strand prepared from normal 48BR cells by PCR, and then sub-cloned into pLenti6.3/V5-D-TOPO vector with sequences encoding a C-terminal V5 tag. HEK293FT cells were transfected with these plasmids one by one, together with ViraPower packaging mix containing pLP1, pLP2 and pLP/VSVG plasmids, using Lipofectamine 2000 (Invitrogen). Viral particles were collected 48 h after transfection and concentrated with PEG-it virus precipitation Solution (System Biosciences).

PROCEDURE

Simultaneous UDS and RRS assays ● TIMING 24–26 h for UDS assay; 34–36 h for RRS assay

1| *Cell seeding*. Prewarm the medium to 37 °C before use. Usually, 5 ml of PBS, 1 ml of 0.05% (wt/vol) trypsin-EDTA and 10 ml of DMEM containing 10% (vol/vol) FBS and 1× penicillin-streptomycin (10% (vol/vol) FBS-DMEM) are sufficient for the processing of one cell strain (**Fig. 2**).

2| Harvest cells from 75-cm^2 plated flasks. Wash the cells once with 5 ml of PBS and incubate them with 1 ml of 0.05% (wt/vol) trypsin-EDTA at 37 °C for 10 min. Then resuspend the cells with 5 ml of 10% (vol/vol) FBS-DMEM. Usually, 4–5 × 10^5 fibroblasts can be harvested from a 175-cm^2 flask.

? TROUBLESHOOTING

3| After counting cell numbers, seed the cells at confluent density (1 × 10^4 cells per well) into a plastic 96-well plate containing 100 µl of 10% (vol/vol) FBS-DMEM (**Fig. 3a**). Incubate the cells at 37 °C with 5% CO_2 for 16–18 h.

▲ **CRITICAL STEP** Cells should be plated at confluent density before UV irradiation to eliminate S-phase cells as much as possible.

4| *UVC irradiation*. Prewarm the medium to 37 °C before use. Wash the cells once with 200 μl of PBS, and add fresh 200 μl of PBS into all plated wells.

5| As shown in **Figure 3a**, split the plate into two groups: wells on the left side are used for UV irradiation (UV+ wells), whereas wells on the right side are used for mock treatment (UV− wells). From UV+ wells, aspirate 200 μl of PBS and keep the remaining UV− wells protected from UV light by wrapping the plate in aluminum foil.

6| Perform EdU incorporation (for UDS assay, option A) or EU incorporation (for RRS assay, option B).

(A) UDS assay

(i) Irradiate the UV+ wells with 20 J/m^2 UVC.

(ii) In the UV+ wells, add 60 μl of serum-free DMEM supplemented with 5 μM EdU immediately after UV irradiation.

(iii) From the UV− wells, aspirate 200 μl of PBS and add 60 μl of serum-free DMEM supplemented with 5 μM EdU.

▲ **CRITICAL STEP** As FBS in culture medium will affect the efficiency of EdU incorporation, remove the culture medium as completely as possible before EdU incorporation.

(iv) Incubate the plate for 4 h at 37 °C with 5% CO_2.

(B) RRS assay

(i) Irradiate the UV+ wells with 11 J/m^2 UVC.

(ii) Add 100 μl of DMEM containing 1% (vol/vol) FBS and 1× penicillin-streptomycin (1% (vol/vol) FBS-DMEM) immediately after UV irradiation.

▲ **CRITICAL STEP** Uridine in FBS will diminish the EU incorporation efficiency; therefore, use DMEM containing 1% (vol/vol) FBS to reduce the amount of uridine in the medium without causing cell death.

(iii) From the UV− wells, aspirate 200 μl of PBS and add 100 μl of 1% (vol/vol) FBS-DMEM.

(iv) Incubate the plate for 12 h at 37 °C with 5% CO_2.

(v) *EU incorporation and detection*. Prewarm the medium to 37 °C. Wash the cells once with 200 μl of PBS, and then add 60 μl of serum-free DMEM supplemented with 100 μM EU.

▲ **CRITICAL STEP** As FBS in culture medium will affect the efficiency of EU incorporation, remove the culture medium as completely as possible before EU incorporation.

(vi) Incubate the plate for 2 h at 37 °C with 5% CO_2.

? TROUBLESHOOTING

7| *Fixation and permeabilization*. Wash the cells once with 200 μl of PBS and then incubate them with 100 μl of fix buffer A for 20 min on ice.

8| Wash the cells three times with 200 μl of PBS at room temperature.

■ **PAUSE POINT** The plate can be stored at 4 °C for up to 2–3 d.

9| Block the cells for 30 min at room temperature with 100 μl of PBS containing 10% (vol/vol) FBS.

10| *Azide-coupling reaction*. Add 40 μl of azide-coupling solution to the cells and incubate them for 1 h at room temperature.

▲ **CRITICAL STEP** The azide-coupling solution must be prepared no more than 5–10 min before use to avoid fluorescence fading.

▲ **CRITICAL STEP** Perform Steps 10–16 in the dark to prevent fluorescence fading.

? TROUBLESHOOTING

11| Wash the cells three times with 200 μl of PBST at room temperature.

12| *DAPI staining*. Incubate the cells with 50 μl of DAPI solution (final concentration of 20 ng/ml in PBS) for 20 min at room temperature.

13| Wash the cells three times with 200 μl of PBST at room temperature.

14| Fix the cells for 20 min at room temperature with 100 μl of fix buffer B.

15| Aspirate the fix buffer and add 200 μl of PBS to the wells with cells and to adjacent wells.

16| *Image acquisition*. Acquire images using an HCS system (option A; see **Supplementary Method 1** and **Supplementary Notes 1** and **2**) or using a standard microscope equipped with a long-working-distance (LD) lens and a CCD camera, and ImageJ (from the US National Institutes of Health, NIH) software (option B; full details in **Supplementary Method 2**).

▲ **CRITICAL STEP** Read the plate immediately if possible or within 48 h (plates should be stored at 4 °C in the dark) as fluorescence fades quickly.

(A) HCS system

(i) Acquire plate images on a HCS system using a 10× or 20× objective lens. If you are using the VTI system, use the Cellomics Target Activation V4 bioapplication program for the UDS assay, or the Cellomics Colocalization V4 bioapplication program for the RRS assay.

(ii) Set the channel parameters for DAPI (channel 1 for nuclei detection) and for Alexa Fluor 488 (channel 2 for the measurement of UDS or RRS activity and channel 3 for nucleolus subtraction in RRS assay).

(iii) For the UDS assay, select an appropriate intensity cutoff level for channel 2 to exclude high-intensity S-phase cells. Readout features must include the cell number (ValidObjectCount) and the average nuclear intensity (MEAN_AvgIntenCh2). For the RRS assay, define ROI_A_Target_I for Alexa Fluor 488 fluorescence signal in the nuclei region (channel 2) and exclude nucleoli (channel 3). Readout features must include the cell number (ValidObjectCount) and the average intensity (MEAN_ROI_A_Target_I_ObjectAvgInten).

(iv) Collect 20–25 field images per well.

(v) Perform data analysis using Microsoft Excel (**Supplementary Method 1**).

(B) Standard microscope equipped with LD lens and a CCD camera, and ImageJ software

(i) Use a standard microscope equipped with an LD lens and a CCD camera, and ImageJ software for image acquisition and nuclear fluorescence intensity measurement.

(ii) Capture appropriate numbers of field images (10× objective) for DAPI and Alexa Fluor 488 staining in each well. Export the images to 8-bit TIFF files for further data processing.

(iii) Use an appropriate ImageJ macro (UDS3Macro, available from the authors) to measure the Alexa Fluor 488 signal intensity in each nucleus.

(iv) Perform data analysis using Microsoft Excel (**Supplementary Method 2**).

? TROUBLESHOOTING

? TROUBLESHOOTING

Troubleshooting advice can be found in **Table 2**.

TABLE 2 | Troubleshooting table.

Step	Problem	Possible reason	Solution
2	Fibroblast cells do not detach from tissue culture flasks	Strong cell adhesion to culture flasks	Extend incubation time with the trypsin-EDTA solution up to 30 min
		Trypsin-EDTA solution is not warm or is inactive	Prewarm the solution at 37 °C before use; use fresh reagents
6B(vi); **Box 1**, steps 3–7	Cells are detached from plates	Washing step is not performed gently enough Cells are dried up during UV-irradiation step	All the wash steps should be performed very gently Minimize exposure of the cells to air during the UV-irradiation process
10	Precipitation appears during preparation of the azide coupling solution	Mixing of the solution is insufficient	Add components in the correct order: first, mix H_2O, Tris-HCl buffer and $CuSO_4$, then add sodium ascorbate and mix well; finally, add Alex Fluor 488–azide. Mix thoroughly after each addition
16	No or weak signal of Alexa Fluor 488	Insufficient incorporation of EdU or EU (Step 6 in main PROCEDURE)	Ensure that media do not contain FBS for EdU or EU incorporation steps; wash cells gently but thoroughly before EdU or EU incorporation
		Insufficient permeabilization (Step 7 in main PROCEDURE)	Make fresh fix and permeabilization buffers
		Overblocking (Step 9 in main PROCEDURE)	The blocking step must be exactly 30 min

(continued)

TABLE 2 | Troubleshooting table (continued).

Step	Problem	Possible reason	Solution
16		Fluorescence fading (Step 10 in main PROCEDURE)	Keep assay plates in the dark after the azide-coupling step; make sure to use freshly prepared azide coupling solution; check pH of the Tris-HCl buffer (pH 7.3); read assay plates as soon as possible
	High background noise during image acquisition	Washing step is insufficient	Wash gently but thoroughly; use an aspirator and 200 μl tips to completely remove media or solutions from 96-well plates
	Diverse numbers of cells in fields	Cells are not plated uniformly (Step 3 in main PROCEDURE)	Pipetting with a multichannel pipette is needed to obtain a homogenous cell resuspension; place a pipette tip along with one side of the well-wall and add cell resuspension medium into a plastic 96-well plate; seed cells in a dropwise manner into a glass-bottomed 96-well plate
16; **Box 2**, step 5B(x)	No or weak DAPI signal	Insufficient permeabilization (Step 7 in main PROCEDURE, step 5B(i) in **Box 2**)	Make fresh buffers for fixing and permeabilization
		Insufficient staining (Step 12 in main PROCEDURE, step 5B(vi) in **Box 2**)	Increase the DAPI concentration
Box 2, step 5B(x)	No or weak Alexa Fluor 488 signal	Insufficient staining (steps 5B(iv,vi) in **Box 2**)	Increase the amount of antibody or consider a longer incubation time
		The primary and the secondary antibodies are incompatible	Check the primary and secondary antibodies used for immunofluorescence
		Poor virus infection efficiency (step 2 in **Box 2**)	Check the viral titer used for infection experiments
	High background	Insufficient blocking (step 5B(iii) in **Box 2**)	Use different blocking reagents
		Antibody concentration may be too high (step 5B(iv,vi) in **Box 2**)	Use a lower antibody concentration
		Washing step is insufficient	Wash gently but thoroughly; use an aspirator and 200 μl tips to completely remove media or solutions from 96-well plates

● TIMING

The UDS assay (Step 6A of the main PROCEDURE) can be completed within 2 d from preparation of assay plates. The RRS assay (Step 6B of the main PROCEDURE) and cell sensitivity assay (**Box 1**) can be completed within 3 d. To confirm the complementation groups, the assays take either 5 d (virus complementary assay; **Box 2**) or 4 d (RNA interfere assay; **Box 3**).

Box 1 | Cell sensitivity assay after UV irradiation (perform this assay if UDS and RRS are normal) ● TIMING 48–50 h

1. *Cell seeding*. Perform Steps 1–3 of the main PROCEDURE (**Figs. 3d** and **5a**).
2. *UV irradiation*. Perform Step 4 of the main PROCEDURE.
3. As shown in **Figure 3d**, the plate is split into four groups: 0 J wells, 5 J wells, 10 J wells and 20 J wells. From 20 J wells, aspirate 200 μl of PBS and keep the remaining wells protected from UV light by wrapping in aluminum foil.

? TROUBLESHOOTING

4. Irradiate the UV+ wells with 20 J/m^2 UVC.

? TROUBLESHOOTING

5. Add 100 μl of 10% (vol/vol) FBS-DMEM immediately after UV irradiation.

? TROUBLESHOOTING

6. Repeat steps 3–5 of this procedure to irradiate the plate with 10 and 5 J/m^2 UVC.

? TROUBLESHOOTING

(continued)

Box 1 | (continued)

7. From the 0 J wells, aspirate 200 µl of PBS, and then add 100 µl of 10% (vol/vol) FBS-DMEM.
? TROUBLESHOOTING
8. Incubate for 24 h at 37 °C with 5% CO_2.
9. *EdU incorporation*. Prewarm the medium to 37 °C before use. Wash cells once with 200 µl of PBS and then add 60 µl of serum-free DMEM supplemented with 5 µM EdU.
▲ **CRITICAL STEP** FBS in culture medium will affect the efficiency of EdU incorporation, so remove medium as completely as possible before EdU incorporation.
10. Incubate cells for 4 h at 37 °C with 5% CO_2.
11. Perform Steps 7–16 of the main PROCEDURE. Note that the Cellomics Target Activation V4 bioapplication program is used for image acquisition and data processing, and no cutoff level for channel 2 is set (**Supplementary Method 1** and **Supplementary Note 3**).

ANTICIPATED RESULTS

Typical results of UDS and RRS assays are shown in **Figure 4**. For these example, normal 48BR, XP patient–derived XP15BR and XP21BR, and CS patient–derived CS2AW cells were seeded on plastic 96-well plates and irradiated with UVC (for UDS,

Box 2 | Virus complementation assay (for determination of complementation groups) ● TIMING 96–98 h

1. *Cell seeding*. Perform Steps 1–3 of the main PROCEDURE (**Figs. 3b–d** and **5**).
2. *Lentivirus infection*. Prewarm the medium to 37 °C before use. Prepare viral solution by mixing an appropriate lentivirus stock solution and polybrene (final concentration 6 ng/µl) in 10% (vol/vol) FBS-DMEM.
3. Add 60 µl of viral solution into 96-well plates. Incubate at 37 °C with 5% CO_2 for at least 24 h.
4. Wash cells once with 200 µl of PBS and then incubate with 100 µl of 10% (vol/vol) FBS-DMEM at 37 °C with 5% CO_2 for 24–48 h.
! CAUTION The series of experiments have a risk of potentially hazardous viral infection to a researcher. Follow local rules and safety regulations. Make sure to wear proper protective clothing and perform the experiments using specific equipment under a safety cabinet. After completion of the experiments, all laboratory bench surfaces, waste media, plastic waste and equipment should be decontaminated according to institutional and governmental guidelines.
5. Split cells into two groups: one to undergo UDS, RRS or cell sensitivity assay, and the other to undergo fixation, permeabilization, staining and image acquisition to determine viral infection efficiency.
(A) UDS, RRS or cell sensitivity assay
(i) The following procedures, including UV irradiation, EdU or EU incorporation, and image acquisition and data analysis steps are the same as described in the main PROCEDURE and **Box 1**. For the UDS assay, perform Steps 4–16 of the main PROCEDURE with Step 6A. For the RRS assay, perform Steps 4–16 of the main PROCEDURE with Step 6B. For the cell sensitivity assay, perform steps 2–11 of **Box 1**). Note that the EdU or EU incorporation is carried out 72 h after viral infection, and the UV-irradiation step for RRS assay (Step 6B of the main PROCEDURE) is carried out 12 h before EU incorporation; the UV-irradiation step for cell sensitivity assay (step 2 of **Box 1**) is carried out 24 h before EdU incorporation.
(B) Determination of viral infection efficiency
(i) *Fixation and permeabilization*. Wash cells once with 200 µl of PBS and then incubate cells with 100 µl of fix buffer C for 30 min on ice.
(ii) Wash cells three times with 200 µl of PBS at room temperature.
■ **PAUSE POINT** The plate can be stored at 4 °C for up to 2–3 d.
(iii) Block the cells for 30 min at room temperature with 100 µl of PBS containing 10% (vol/vol) FBS.
(iv) *Primary antibody incubation*. Aspirate 100 µl of PBS and add 40 µl of anti–V5-tag mouse monoclonal antibody solution (antibody diluted in PBST at 1:250) and incubate the cells for 1 h at room temperature.
(v) Wash the cells three times with 200 µl of PBST at room temperature.
(vi) *Secondary antibody incubation*. Aspirate 200 µl of PBST and add 40 µl of secondary antibody solution (Alexa Fluor 488–conjugated goat anti-mouse IgG; diluted in PBST at 1:1,000 with 10 ng/ml DAPI). Incubate the cells for 1 h at room temperature. Alternatively, DAPI staining can be separately performed after washing.
(vii) Wash the cells three times with 200 µl of PBST at room temperature.
(viii) Fix the cells for 20 min at room temperature with 100 µl of fix buffer B.
(ix) Aspirate the fix buffer and add 200 µl of PBS in the wells with cells and in surrounding wells.
(x) Image acquisition using an HCS system. Follow Step 16 of the main PROCEDURE. Note that reference wells must be set as wells without infection control, and readout features must include cell number (ValidObjectCount), average nuclear intensity (MEAN_AvgIntenCh2), s.d. of average intensity (SD_AvgIntenCh2) and percentage of cells with average intensity above high-response level (%Responders_ AvgIntenCh2).
▲ **CRITICAL STEP** Read the plates immediately if possible or within 48 h (the plate should be stored at 4 °C in the dark) as fluorescence fades quickly.
? TROUBLESHOOTING

Box 3 | RNA interference assay (for confirmation of pathogenic candidate genes) ● TIMING 80–82 h

1. *Cell seeding*. Perform Steps 1 and 2 of the main PROCEDURE (**Fig. 5c**).
2. *Prepare siRNA transfection mixture*. Mix an appropriate siRNA stock solution (final concentration 10 nM) and X-tremeGENE transfection reagent with 20 µl of serum-free DMEM according to the manufacturer's instructions. The siRNA transfection mixture is incubated for 15 min at room temperature in a 96-well plate.
3. Count cell numbers and add 1×10^4 cells (suspended in 80 µl of 10% (vol/vol) FBS-DMEM) into the 96-well plate containing siRNA transfection mixture (**Fig. 3f**). Incubate the cells at 37 °C with 5% CO_2 for 72 h to allow for knockdown of target gene expression.
4. *UDS and RRS assay*. Perform Steps 4–16 of the main PROCEDURE. Note that the UV-irradiation step for RRS assay (Step 6B of the main PROCEDURE) is carried out with 9 J/m², followed with 4 h of incubation in 1% (vol/vol) FBS-DMEM.

20 J/m² UVC; for RRS, 11 J/m² UVC). *XPA*-deficient XP15BR should show a very low level of UDS and RRS activity. XP21BR, which is compromised only in GGR because of *XPC* deficiency, should display low-level activity in UDS but retain nearly normal activity in RRS, whereas *CSA*-deficient CS2AW, which is compromised only in TCR, should exhibit reduced RRS activity but almost normal UDS levels. As shown in **Figure 6a,b**, reduced UDS or RRS activity after UV irradiation should be completely restored by the infection of lentivirus expressing *XPA* in XP15BR, *XPC* in XP21BR, or *CSA* in CS2AW. The expression of V5-tagged protein can be confirmed by fluorescence microscopy (**Fig. 6c**), and viral infection efficiency can be calculated using the VTI system (**Fig. 6d**). The RNA interference assay should confirm that both UDS and RRS activities are reduced after knockdown of the *XPA* gene expression by siRNA transfection, whereas only RRS activity is reduced after knockdown of the *UVSSA* gene expression (**Fig. 8**).

Figure 7 demonstrates typical results of the cell sensitivity assay. For this example, normal 48BR, and NER-deficient XP15BR, XP21BR and CS2AW cells were seeded on a plastic 96-well plate and irradiated with different doses of UVC (0, 5, 10 and 20 J/m²). Cell viability was measured by their ability to incorporate EdU 24 h after UV irradiation. As shown in **Figure 7a**, cells derived from XP or CS patients were more sensitive to UV irradiation compared with normal cells. Ectopic expression of *XPA* in XP15BR, *XPC* in XP21BR or *CSA* in CS2AW by lentivirus infection restored the cell viability to nearly normal level. Fluctuations and statistical data from past assays (n = 3–25; data collected from published[15,32,34] and unpublished in-house experiments (Y. Nazakawa and N.J., unpublished data)) are shown in **Supplementary Figure 5** and **Supplementary Tables 1–3**. The results are reproducible and fluctuations between experiments are small.

Note: Any Supplementary Information and Source Data files are available in the online version of the paper.

ACKNOWLEDGMENTS We are grateful to H. Niki for his support with the project. This work was supported by Special Coordination Funds for Promoting Science and Technology from Japan Science and Technology Agency, KAKENHI Grants-in-Aid for Young Scientists B (24790321) from the Japan Society for the Promotion of Science (JSPS), a cancer research grant from The Sagawa Foundation for Promotion of Cancer Research, the Sasakawa Scientific Research Grant from the Japan Science Society, a medical research grant from Mochida Memorial Founds for Medical and Pharmaceutical Research and a science research grant from Inamori Foundation to Y. Nakazawa; KAKENHI Grants-in-Aids for Young Scientists A (24681008) and for Exploratory Research (24659533) from JSPS, a grant for Health Labour Sciences Research (26310301) from The Ministry of Health Labour and Welfare, a research grant from The Kanae Foundation for the Promotion of Medical Science, a basic science research grant from The Sumitomo Foundation, a basic research grant from The Nakatomi Foundation, a research grant from Suzuken Memorial Foundation, a science research grant from Ube Industries Foundation for Promotion of Science, a science research grant from The Uehara Memorial Foundation to T.O.; KAKENHI Grants-in-Aid for Young Scientists B (25870534) from JSPS to C.G.; and the project is partly supported by Platform for Drug Discovery, Informatics and Structural Life Science from the Ministry of Education, Culture, Sports, Science and Technology, Japan.

AUTHOR CONTRIBUTIONS Y. Nakazawa and T.O. designed the study; N.J. and Y. Nakazawa optimized all the experimental protocols; N.J., Y. Nakazawa, C.G., M. Shimada and M. Sethi performed the experiments; Y.T., H.U., Y. Nagayama and T.O. coordinated the study; N.J. and T.O. wrote the manuscript; and all authors commented on the manuscript.

COMPETING FINANCIAL INTERESTS
The authors declare competing financial interests: details are available in the online version of the paper.

1. Hoeijmakers, J.H. Genome maintenance mechanisms for preventing cancer. *Nature* **411**, 366–374 (2001).
2. Friedberg, E.C. *et al. DNA Repair and Mutagenesis* 2nd edn. (ASM Press, 2005).
3. Lehmann, A.R. DNA repair-deficient diseases, xeroderma pigmentosum, Cockayne syndrome and trichothiodystrophy. *Biochimie* **85**, 1101–1111 (2003).
4. de Boer, J. & Hoeijmakers, J.H. Nucleotide excision repair and human syndromes. *Carcinogenesis* **21**, 453–460 (2000).
5. Kraemer, K.H. *et al.* Xeroderma pigmentosum, trichothiodystrophy and Cockayne syndrome: a complex genotype-phenotype relationship. *Neuroscience* **145**, 1388–1396 (2007).
6. Shuck, S.C., Short, E.A. & Turchi, J.J. Eukaryotic nucleotide excision repair: from understanding mechanisms to influencing biology. *Cell Res.* **18**, 64–72 (2008).
7. Gillet, L.C. & Scharer, O.D. Molecular mechanisms of mammalian global genome nucleotide excision repair. *Chem. Rev.* **106**, 253–276 (2006).
8. Vermeulen, W. & Fousteri, M. Mammalian transcription-coupled excision repair. *Cold Spring Harb. Perspect. Biol.* **5**, a012625 (2013).
9. Hanawalt, P.C. & Spivak, G. Transcription-coupled DNA repair: two decades of progress and surprises. *Nat. Rev. Mol. Cell Biol.* **9**, 958–970 (2008).
10. Stefanini, M., Fawcett, H., Botta, E., Nardo, T. & Lehmann, A.R. Genetic analysis of twenty-two patients with Cockayne syndrome. *Hum. Genet.* **97**, 418–423 (1996).
11. Kleijer, W.J. *et al.* Incidence of DNA repair deficiency disorders in western Europe: xeroderma pigmentosum, Cockayne syndrome and trichothiodystrophy. *DNA Repair (Amst)* **7**, 744–750 (2008).

12. Masutani, C. *et al.* The *XPV* (xeroderma pigmentosum variant) gene encodes human DNA polymerase eta. *Nature* **399**, 700–704 (1999).
13. Naegeli, H. & Sugasawa, K. The xeroderma pigmentosum pathway: decision tree analysis of DNA quality. *DNA Repair (Amst)* **10**, 673–683 (2011).
14. Egly, J.M. & Coin, F. A history of TFIIH: two decades of molecular biology on a pivotal transcription/repair factor. *DNA Repair (Amst)* **10**, 714–721 (2011).
15. Nakazawa, Y. *et al.* Mutations in *UVSSA* cause UV-sensitive syndrome and impair RNA polymerase IIo processing in transcription-coupled nucleotide-excision repair. *Nat. Genet.* **44**, 586–592 (2012).
16. Schwertman, P. *et al.* UV-sensitive syndrome protein UVSSA recruits USP7 to regulate transcription-coupled repair. *Nat. Genet.* **44**, 598–602 (2012).
17. Zhang, X. *et al.* Mutations in *UVSSA* cause UV-sensitive syndrome and destabilize ERCC6 in transcription-coupled DNA repair. *Nat. Genet.* **44**, 593–597 (2012).
18. Lehmann, A.R. The xeroderma pigmentosum group D (*XPD*) gene: one gene, two functions, three diseases. *Genes Dev.* **15**, 15–23 (2001).
19. Kraemer, K.H. From proteomics to disease. *Nat. Genet.* **36**, 677–678 (2004).
20. Scharer, O.D. Hot topics in DNA repair: the molecular basis for different disease states caused by mutations in *TFIIH* and *XPG*. *DNA Repair (Amst)* **7**, 339–344 (2008).
21. Ahmad, A. *et al.* Mislocalization of XPF-ERCC1 nuclease contributes to reduced DNA repair in XP-F patients. *PLoS Genet.* **6**, e1000871 (2010).
22. Mayne, L.V. & Lehmann, A.R. Failure of RNA synthesis to recover after UV irradiation: an early defect in cells from individuals with Cockayne's syndrome and xeroderma pigmentosum. *Cancer Res.* **42**, 1473–1478 (1982).
23. Stefanini, M. *et al.* Genetic heterogeneity of the excision repair defect associated with trichothiodystrophy. *Carcinogenesis* **14**, 1101–1105 (1993).
24. Lehmann, A.R. & Stevens, S. A rapid procedure for measurement of DNA repair in human fibroblasts and for complementation analysis of xeroderma pigmentosum cells. *Mutat. Res.* **69**, 177–190 (1980).
25. Lehmann, A.R., Thompson, A.F., Harcourt, S.A., Stefanini, M. & Norris, P.G. Cockayne's syndrome: correlation of clinical features with cellular sensitivity of RNA synthesis to UV irradiation. *J. Med. Genet.* **30**, 679–682 (1993).
26. Hashimoto, S., Egawa, K., Ihn, H. & Tateishi, S. Non-radioisotope method for diagnosing photosensitive genodermatoses and a new marker for xeroderma pigmentosum variant. *J. Dermatol.* **36**, 138–143 (2009).
27. Protic-Sabljic, M. & Kraemer, K.H. Host cell reactivation by human cells of DNA expression vectors damaged by ultraviolet radiation or by acid-heat treatment. *Carcinogenesis* **7**, 1765–1770 (1986).
28. Salic, A. & Mitchison, T.J. A chemical method for fast and sensitive detection of DNA synthesis *in vivo*. *Proc. Natl. Acad. Sci. USA* **105**, 2415–2420 (2008).
29. Jao, C.Y. & Salic, A. Exploring RNA transcription and turnover *in vivo* by using click chemistry. *Proc. Natl. Acad. Sci. USA* **105**, 15779–15784 (2008).
30. Kolb, H.C., Finn, M.G. & Sharpless, K.B. Click chemistry: diverse chemical function from a few good reactions. *Angew. Chem. Int. Ed. Engl.* **40**, 2004–2021 (2001).
31. Limsirichaikul, S. *et al.* A rapid non-radioactive technique for measurement of repair synthesis in primary human fibroblasts by incorporation of ethynyl deoxyuridine (EdU). *Nucleic Acids Res.* **37**, e31 (2009).
32. Nakazawa, Y., Yamashita, S., Lehmann, A.R. & Ogi, T. A semi-automated non-radioactive system for measuring recovery of RNA synthesis and unscheduled DNA synthesis using ethynyluracil derivatives. *DNA Repair (Amst)* **9**, 506–516 (2010).
33. Ogi, T. *et al.* Three DNA polymerases, recruited by different mechanisms, carry out NER repair synthesis in human cells. *Mol. Cell* **37**, 714–727 (2010).
34. Kashiyama, K. *et al.* Malfunction of nuclease ERCC1-XPF results in diverse clinical manifestations and causes Cockayne syndrome, xeroderma pigmentosum, and Fanconi anemia. *Am. J. Hum. Genet.* **92**, 807–819 (2013).
35. Woodbine, L. *et al.* *PRKDC* mutations in a SCID patient with profound neurological abnormalities. *J. Clin. Invest.* **123**, 2969–2980 (2013).
36. Arlett, C.F., Green, M.H., Priestley, A., Harcourt, S.A. & Mayne, L.V. Comparative human cellular radiosensitivity: I. The effect of SV40 transformation and immortalisation on the gamma-irradiation survival of skin derived fibroblasts from normal individuals and from ataxia-telangiectasia patients and heterozygotes. *Int. J. Radiat. Biol.* **54**, 911–928 (1988).
37. Arlett, C.F. *et al.* Clinical and cellular ionizing radiation sensitivity in a patient with xeroderma pigmentosum. *Br. J. Radiol.* **79**, 510–517 (2006).
38. Ren, Y. *et al.* Three novel mutations responsible for Cockayne syndrome group A. *Genes Genet Syst.* **78**, 93–102 (2003).

Research article

Hypomorphic PCNA mutation underlies a human DNA repair disorder

Emma L. Baple,[1] Helen Chambers,[2] Harold E. Cross,[3] Heather Fawcett,[4] Yuka Nakazawa,[5,6] Barry A. Chioza,[1] Gaurav V. Harlalka,[1] Sahar Mansour,[7] Ajith Sreekantan-Nair,[1] Michael A. Patton,[1] Martina Muggenthaler,[1] Phillip Rich,[8] Karin Wagner,[9] Roselyn Coblentz,[9] Constance K. Stein,[10] James I. Last,[11] A. Malcolm R. Taylor,[11] Andrew P. Jackson,[12] Tomoo Ogi,[5,6] Alan R. Lehmann,[4] Catherine M. Green,[2,13] and Andrew H. Crosby[1]

[1]Medical Research, RILD Wellcome Wolfson Centre, University of Exeter Medical School, Exeter, Devon, United Kingdom. [2]Department of Zoology, University of Cambridge, Cambridge, United Kingdom. [3]Department of Ophthalmology, University of Arizona College of Medicine, Tucson, Arizona, USA. [4]Genome Damage and Stability Centre, University of Sussex, Falmer, Brighton, United Kingdom. [5]Nagasaki University Research Centre for Genomic Instability and Carcinogenesis (NRGIC), Nagasaki, Japan. [6]Department of Molecular Medicine, Atomic Bomb Disease Institute, Nagasaki University, Nagasaki, Japan. [7]SW Thames Regional Genetics Service, St. George's Healthcare NHS Trust, London, United Kingdom. [8]Department of Neuroradiology, St. George's Hospital, London, United Kingdom. [9]Windows of Hope Genetic Study, Walnut Creek, Ohio, USA. [10]SUNY Upstate Medical University, Syracuse, New York, USA. [11]School of Cancer Sciences, College of Medical and Dental Sciences, University of Birmingham, Birmingham, United Kingdom. [12]MRC Human Genetics Unit, Institute of Genetics and Molecular Medicine, University of Edinburgh, Edinburgh, United Kingdom. [13]Wellcome Trust Centre for Human Genetics, University of Oxford, Oxford, United Kingdom.

Numerous human disorders, including Cockayne syndrome, UV-sensitive syndrome, xeroderma pigmentosum, and trichothiodystrophy, result from the mutation of genes encoding molecules important for nucleotide excision repair. Here, we describe a syndrome in which the cardinal clinical features include short stature, hearing loss, premature aging, telangiectasia, neurodegeneration, and photosensitivity, resulting from a homozygous missense (p.Ser228Ile) sequence alteration of the proliferating cell nuclear antigen (PCNA). PCNA is a highly conserved sliding clamp protein essential for DNA replication and repair. Due to this fundamental role, mutations in PCNA that profoundly impair protein function would be incompatible with life. Interestingly, while the p.Ser228Ile alteration appeared to have no effect on protein levels or DNA replication, patient cells exhibited marked abnormalities in response to UV irradiation, displaying substantial reductions in both UV survival and RNA synthesis recovery. The p.Ser228Ile change also profoundly altered PCNA's interaction with Flap endonuclease 1 and DNA Ligase 1, DNA metabolism enzymes. Together, our findings detail a mutation of PCNA in humans associated with a neurodegenerative phenotype, displaying clinical and molecular features common to other DNA repair disorders, which we showed to be attributable to a hypomorphic amino acid alteration.

Introduction

Maintenance of genomic integrity is fundamentally important for normal cell division and basic cellular biological processes. The molecular characterization of human DNA damage sensitivity disorders, such as ataxia telangiectasia (AT), xeroderma pigmentosum (XP), and Cockayne syndrome (CS), has provided unique insight into the cellular mechanisms required for DNA damage tolerance and repair, and their importance for human health. The key features of such syndromes include predisposition to premature aging, malignancy, neurodegeneration, immunodeficiency, photosensitivity, and growth insufficiency (1–4). The process of nucleotide excision repair (NER) consists of 2 DNA repair pathways that are crucial for the removal of bulky lesions in DNA, including photoproducts resulting from exposure to UV light. Transcription-coupled NER (TC-NER) rapidly undertakes preferential repair of DNA lesions on actively transcribed DNA strands and is deficient in CS and UV-sensitive syndrome (5). Global genome NER (GG-NER) removes photoproducts more slowly from across the genome and is deficient in XP and trichothiodystrophy (6). After DNA damage is detected, both NER processes involve the excision of about 30 nucleotides encompassing the damaged DNA, followed by repair synthesis of new DNA to replace the damaged section. Repair synthesis is absolutely dependent on the DNA polymerase accessory protein proliferating cell nuclear antigen (PCNA) (7). This protein's major cellular role is to recruit and retain the replicative DNA polymerases at the sites of DNA synthesis during DNA replication. It forms a homotrimeric ring encircling and freely sliding along the DNA helix. PCNA interacts with a large number of accessory proteins and acts as a protein recruitment platform to coordinate the multiple enzymatic activities required for DNA replication and repair (8).

In the current study, 4 individuals aged 11–31 years affected by a novel syndrome were identified from a single extended pedigree consisting of 2 kindreds within the Ohio Amish community (Figure 1). The principal features included neurodegeneration, postnatal growth retardation, prelingual sensorineural hearing loss, premature aging, ocular and cutaneous telangiectasia, learning difficulties, photophobia, and photosensitivity with evidence of predisposition to sun-induced malignancy. Phenotypic similarities with XP, CS, and AT were noted (Table 1). All 4 affected individuals displayed short stature ranging from −3.8 to −5.2 standard deviation score (SDS), with an absence of pubertal growth spurt in the 2 eldest individuals. Neurodegeneration was a consistent feature,

Conflict of interest: The authors have declared that no conflict of interest exists.
Citation for this article: *J Clin Invest.* 2014;124(7):3137–3146. doi:10.1172/JCI74593.

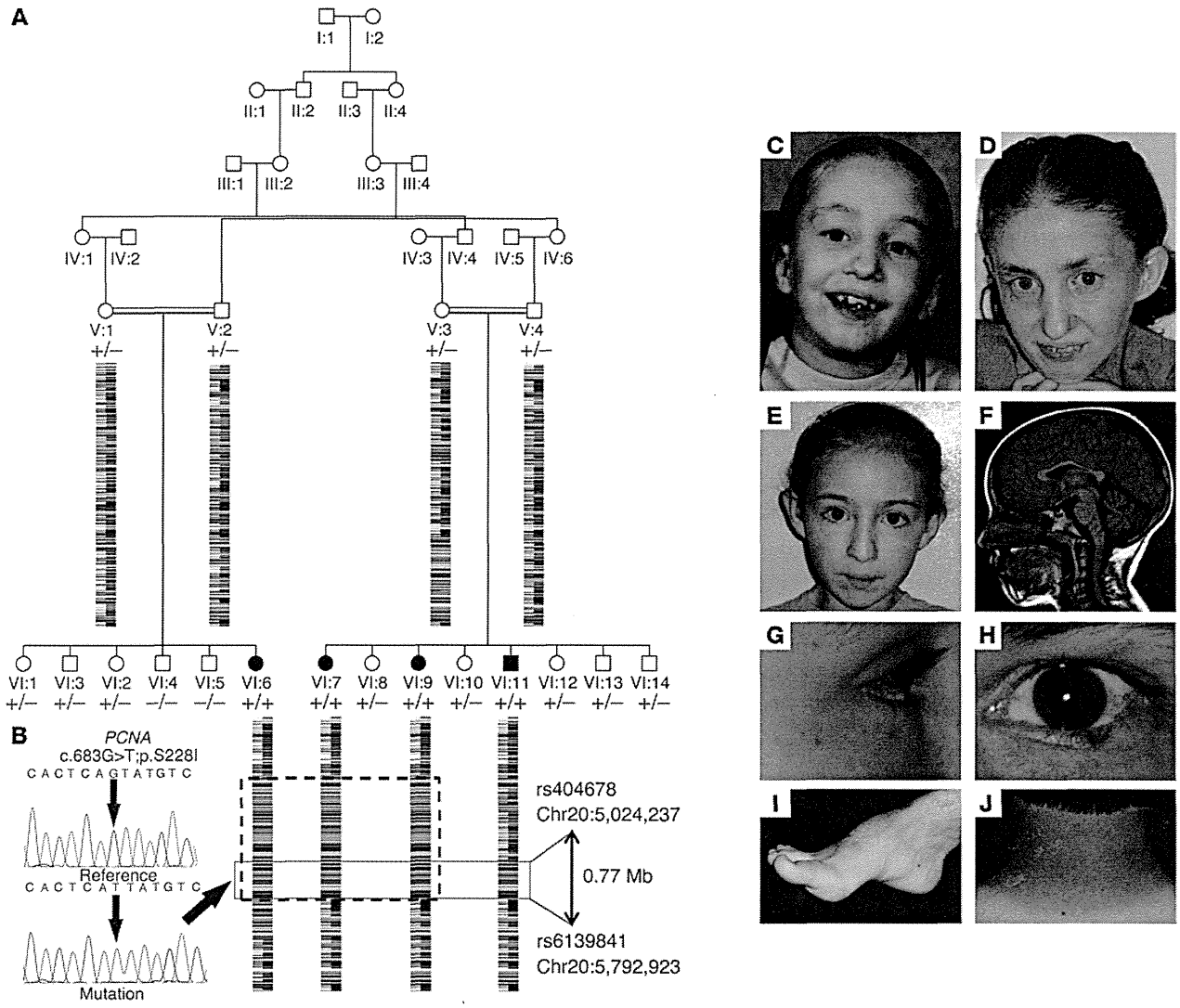

Figure 1

Family pedigree showing *PCNA* c.683G>T genotype data and images of affected individuals. (**A**) Simplified pedigree of the extended Amish family investigated, with pictorial representation of genotypes across ~6 Mb of chromosome 20 encompassing the disease locus (dashed blue boxed region, 2.72-Mb autozygous section in affected females; red boxed region, common 0.77-Mb region). Genotype is shown in red under individuals in generations V and VI (+, mutant; –, WT). All affected individuals were subsequently shown to be homozygous for the *PCNA* variant NM_002592.2 c.683G>T (indicated). Parental samples were heterozygous, and unaffected siblings were either WT or heterozygous carriers. (**B**) Electropherograms showing the DNA sequence at the position of *PCNA* c.683G>T in a WT control and a homozygous affected individual. (**C**–**J**) Clinical features of individuals homozygous for *PCNA* c.683G>T. (**C** and **D**) Patient VI:6 at 8 (**C**) and 31 (**D**) years of age, showing signs of premature aging. (**E**) Patient VI:7 at 11 years of age, with bilateral hearing aids in situ. (**F**) Midline sagittal T1-weighted brain scan of patient VI:9 at 8 years of age. Atrophy of the cerebellar vermis resulted in enlargement of vermian sulci and mild widening of the fourth ventricle. The brainstem was normal in appearance, and no supratentorial abnormality was noted. (**G** and **H**) Ocular and cutaneous telangiectasia in patients VI:7 and VI:11. (**I**) Pes cavus in patient VI:11. (**J**) Photosensitivity after minimal sun exposure in patient VI:11.

characterized by progressive gait instability, muscle weakness, foot deformity, difficulties with speech and swallowing, learning difficulties, and cognitive decline with advancing age. Prelingual onset of moderate to profound (worse at high frequency) sensorineural hearing loss was universal, a feature not commonly associated with the recognized DNA repair defects, and there was clear evidence of progression in patient VI:9. Muscle weakness was progressive; patient VI:6 had been wheelchair bound since the age of 16 years with contractures in all 4 limbs. Speech was unclear from onset and deteriorated with age; at the end of the present study, patient VI:6 had no speech and communicated with basic gestures. Progressive difficulty with swallowing solids/drooling was present in 3 of 4 affected patients. Neuroimaging was only available in 1 case (patient VI:7): MRI of the brain at 8 years of age demonstrated cerebellar atrophy involving the cerebellar vermis and hemispheres. Inner ear abnormalities included bilateral mild labyrinthine dysplasia with mildly dilated vestibules. All patients exhibited photophobia and photosensitivity, with evidence of premalignant changes in

Table 1
Clinical findings of individuals homozygous for *PCNA* c.683G>T and features of AT, CS, and the neurological form of XP

Trait	Patient VI:7	Disease VI:9	VI:11	VI:6	AT	CS	XP (neurological form)[A]
Gender, age (yr)	F, 11.5	F, 14.3	M, 26	F, 31			
Growth							
Short stature	–3.8 SDS	–5.2 SDS	–4.3 SDS	Substantial[B]	+	++	+
Head circumference (OFC)/ microcephaly	–3.2 SDS	–2.8 SDS	0.1 SDS	–2.8 SDS	–	++	+
Eyes							
Ocular telangiectasia	Present	Present	Present	Absent	++	–	–
Photophobia	Present	Present	Present	Present	–	+	++
Other eye abnormalities	Absent	Absent	Absent	UV-induced conjunctivitis	Oculomotor apraxia	Cataracts, pigmentary retinopathy, optic atrophy	UV-induced conjunctivitis, inflammatory lesions (limited to sun-exposed structures)
Skin							
Cutaneous telangiectasia	Present	Present	Present	Present	++	–	–
Photosensitivity	Present	Present	Present	Present	–/+	++	++
Predisposition to sunlight-induced skin cancer	Not known	Not known	Present	Not known	–/+	–	++
Neurology							
Developmental delay/ intellectual disability	Mild	Mild	Mild/ moderate	Severe	–/+	++	++
Ataxia/gait instability	Present	Present	Present	Present	++	++	+
Neurodegeneration	Present	Present	Present	Present	++	++	++
Cerebellar atrophy	Not known	Present	Not known	Not known	++	++[C]	++
Hearing loss	Present[D]	Present[D]	Present[D]	Present[D,E]	–	++[F]	++[F]
Additional features							
Premature aging	Not known	Not known	Absent	Present	+	++	++
Other physical findings	None	None	Absent pubertal growth spurt	Diaphragmatic hernia, absent pubertal growth spurt	Increased risk of leukemia and lymphoma	Incomplete puberty, dental caries	None

++, hallmark of the disease; +, sometimes associated with the disease; –, not associated with the disease. [A]About 25% of XP patients have neurological abnormalities (from groups A, D, F, and G). [B]Not possible to obtain accurate measurement. [C]Also hypomyelination and putaminal calcifications. [D]Prelingual. [E]Cognitive impairment prevented accurate assessment of severity. [F]Progressive, postlingual.

patient VI:11 (basal cell carcinoma in situ). All had several cutaneous telangiectasias, and 3 of 4 had conjunctival telangiectasia.

Assuming that a founder mutation was responsible for the condition, we used a combination of autozygosity mapping and linkage analysis to study this novel syndrome and identify the underlying molecular cause.

Results

A genome-wide SNP microarray scan of DNA from affected individuals and parents was undertaken. Inspection of resultant genotypes identified a single notable region of homozygosity of ~2.72 Mb on chromosome 20p13, shared solely by the 3 affected females. In the affected male, a de novo telomeric recombination event reduced this region to ~0.77 Mb, delimited by markers rs404678 and rs6139841 (NC_000020.10 g.5,024,237–5,792,923; Figure 1), likely to correspond to the disease locus (LOD_{max} 6.4). Microsatellite marker analysis confirmed autozygosity across this region (data not shown). We sequenced all 6 protein coding genes in the region (*PCNA*, *CDS2*, *PROKR2*, *GPCPD1*, *C20orf30*, and *C20orf196*), revealing a single potentially pathogenic sequence variant (NM_002592.2 c.683G>T) in exon 6 of *PCNA*. This variant, which cosegregated with the disease phenotype and was verified in the RNA transcript obtained from whole blood of an affected individual, was predicted to result in a substitution of a stringently conserved serine at position 228 for isoleucine (p.Ser228Ile) (Supplemental Figure 1; supplemental material available online with this article; doi:10.1172/JCI74593DS1). The variant was not detected in 360 control chromosomes of European ancestry, and only 2 heterozygous carriers were detected in the analysis of 310 Ohio Amish control chromosomes, which is not unexpected in this endogamous community. Only a single heterozygous carrier of European origin was identified in online sequencing project databases (1,000 Genomes Project and Exome Variant Server, ESP6500SI release). This single mutation carrier in 7,775 non-Amish individuals genotyped corresponds to a homozygous *PCNA* c.683T allele incidence in the region of approximately 1 in 241 million. We also subjected a single affected individual to whole exome sequence analysis (Otogenetics Corp.) to exclude other possible genetic causes. As expected, this confirmed the presence of the PCNA variant, but identi-

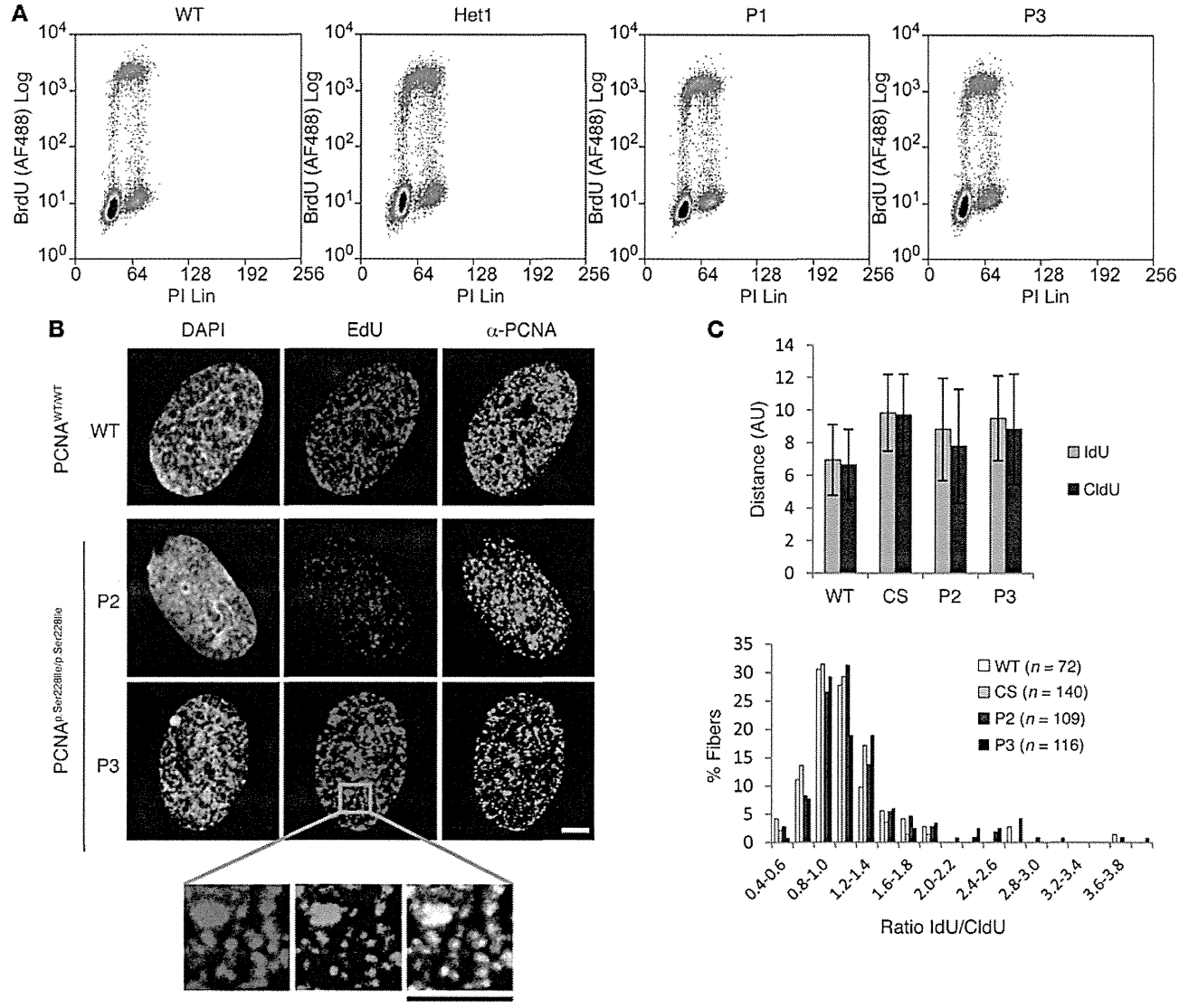

Figure 2

Cells homozygous for PCNA p.Ser228Ile have normal replication parameters. (**A**) FACS analysis of S phase in primary cells. Cells (passage <10) were labeled with BrdU for 30 minutes, and BrdU incorporation and DNA content were analyzed by FACS. No apparent differences were observed between cells from affected individuals (P1 and P3) and related (Het1) or unrelated (WT) control cells. Representative scatter plots are shown; each line was independently analyzed at least twice. (**B**) Immunofluorescence of primary control cells (WT) and affected individuals homozygous for PCNA p.Ser228Ile (P2 and P3). Right: Soluble proteins were removed by triton extraction prior to fixation, and cells were immunostained for PCNA. Middle: Sites of active DNA replication, visible as foci of incorporation of EdU. Enlargement shows colocalization between signals. Left: DNA was counterstained with DAPI. Scale bars: 3 μm. (**C**) Analysis of replication fork progression. Primary control cells, CS cells, and cells homozygous for PCNA p.Ser228Ile (P2 and P3) were incubated sequentially in medium supplemented with IdU and CldU, and the length of the DNA fiber replicated during each pulse was measured. Top: Comparable lengths of DNA were replicated during each pulse. Bottom: Similar frequency distribution of the IdU/CldU ratio within each fiber between cell lines. Error bars indicate SEM of 2 experiments.

fied no other known or possible pathogenic variants elsewhere, after excluding variants not compatible with recessive inheritance or cosegregating with the disease phenotype. Further conclusive support for the exclusion of diagnosis of AT and AT-like disorders was provided by our findings that included normal chromosomes (untreated or γ ray-induced; patient VI:11), alpha-fetoprotein (AFP) levels, Ig patterns (patients VI:7 and VI:9), and ataxia telangiectasia mutated (ATM) and associated protein and kinase activity levels (patients VI:6 and VI:11) in affected subjects (Supplemental Figures 2 and 3).

PCNA is an essential DNA replication accessory protein, highly conserved throughout evolution. It plays a central role at the replication fork, recruiting and retaining many of the enzymes required for DNA replication (8). Due to its fundamentally important cellular role, mutations that substantially affect PCNA protein function would be predicted to result in embryonic lethality. However, the survival of $PCNA^{Lys164Arg/Lys164Arg}$ knockin mice, generated to determine the role of PCNA lysine 164 modifications in somatic hypermutation, demonstrates that certain hypomorphic muta-

tions of PCNA can be tolerated in mammals (9). However, to our knowledge, no inherited human disorder arising from PCNA mutation has been previously described.

We therefore investigated the functional consequences of the PCNA p.Ser228Ile alteration. Primary fibroblasts (P-) were established from 3 affected individuals, patients VI:11, VI:9, and VI:7 (P1, P2, and P3, respectively), 2 heterozygous carriers (Het1 and Het2), and WT controls. EBV-transformed lymphoblastoid cells (L-) were established from 2 affected individuals, patients VI:11 and VI:6 (L5 and L6), 2 carriers (L8 and L10), and 2 Amish WT controls (L7 and L9). PCNA protein levels were unaltered in cells from affected individuals (Supplemental Figure 2). In order to assess the influence of the p.Ser228Ile alteration on DNA replication, we incubated primary fibroblasts (passage <10) with BrdU for 30 minutes and analyzed incorporation and DNA content by FACS (Figure 2A). No apparent differences were observed when comparing the fibroblasts from affected individuals with WT or heterozygote controls. During S phase, PCNA is recruited to so-called "DNA replication factories," the sites of nucleotide incorporation, which are visible as foci in the nuclei of replicating cells. Immunofluorescence analysis of endogenous PCNA in fibroblasts from affected individuals revealed no abnormalities in these foci (Figure 2B). In addition, no difference in replication fork rate was detected during unperturbed S phase using DNA fiber analysis (Figure 2C). Together, these data led us to conclude that the p.Ser228Ile variant does not dramatically interfere with the major replicative function of PCNA and that bulk DNA replication is not grossly perturbed.

Given that repair synthesis and downstream events of NER are absolutely dependent on PCNA (7), the reported photosensitivity in p.Ser228Ile homozygotes prompted us to examine the effect of the p.Ser228Ile substitution on cellular sensitivity to UV. Both primary fibroblasts and lymphoblastoid cells from affected individuals were more sensitive to UV irradiation than cells with WT PCNA (Figure 3, A and B), which suggests that the mutation specifically impairs the function of PCNA in DNA repair. To investigate this further, we evaluated GG-NER in primary fibroblast cell lines, measured by unscheduled DNA synthesis (UDS) assay (10). In cells from affected individuals, UDS was reproducibly reduced to approximately 50%–60% of normal values (Figure 3C). The level of RNA synthesis recovery (RRS) after UV radiation was used as a marker of TC-NER (11, 12). RRS was markedly decreased, to approximately 30%–50% of normal, in cells from affected individuals (Figure 3D and Supplemental Figure 4). The deficiency approached that of CS cells, which are known to be defective in TC-NER. Importantly, ectopic expression of WT PCNA fully rescued the RRS deficiency (Figure 3E), whereas it had only a minor effect on RRS in normal fibroblasts (Supplemental Figure 5), which demonstrated that the deficient UV responses were caused by the p.Ser228Ile sequence alteration. Although the 2 assays for UDS and RRS are by their nature different from each other and are semiquantitative, these results suggest that a subtle alteration in PCNA structure resulting from the p.Ser228Ile substitution is sufficient to specifically disrupt its role in NER, and this appears to have a more substantial effect on TC-NER.

Ser228 lies near the external face of PCNA (Figure 4A), and the mutation is therefore unlikely to affect its interaction with DNA. This residue is also distant from the regions of PCNA that mediate the formation of the trimeric ring structure (13). Consistent with this, no differences in trimer formation or stability between recombinant PCNA WT and p.Ser228Ile proteins were detected using gel filtration or glycerol gradient sedimentation (data not shown), and the amount of chromatin-associated PCNA (resistant to detergent extraction) was similar in WT and p.Ser228Ile homozygous cells. Interestingly, however, the altered residue is close to the interdomain connecting loop (IDCL) region, which mediates the interaction of PCNA with many of its protein partners. PCNA partner proteins, including DNA polymerase delta (PolD), DNA Ligase 1 (Lig1), and Flap endonuclease 1 (Fen1), often contain a PCNA-interacting protein (PIP) box, a sequence motif that mediates the IDCL interaction (14). In published crystal structures, Ser228 does not directly contact the PIP box–containing peptide (13, 15), although its close proximity to the interaction region may generate subtle positional alterations within this crucial domain, with functional consequences.

To determine whether specific protein interactions are perturbed by the p.Ser228Ile alteration, we performed a stable isotope labeling by aas in culture (SILAC) affinity purification assay. Extracts were made from HeLa cells grown in either normal medium or SILAC medium containing "heavy" amino acids ($[^{13}C_6/^{15}N_2]$ lysine and $[^{13}C_6/^{15}N_4]$ arginine). These extracts were individually exposed to affinity columns composed of recombinant PCNA (WT or p.Ser228Ile). Proteins that bound to each column were eluted, the eluates were combined, and the relative binding to each column was determined by mass spectrometry. This identified clear perturbations in the interaction of PCNA p.Ser228Ile with a limited number of interacting partners, most strikingly Fen1 and Lig1 (Figure 4B and Supplemental Table 1). This experiment revealed relatively increased amounts of Fen1 and Lig1 in the 500 mM eluates from the p.Ser228Ile compared with the WT column. To investigate this unexpected finding further, we analyzed the salt resistance of the PCNA-Fen1 interaction. HeLa nuclear extract was incubated with His-tagged PCNA (WT or p.Ser228Ile) beads, which were then washed with increasing NaCl up to 500 mM. The material eluted at 1 M NaCl and that retained on the beads was subsequently analyzed by Western blot for Fen1, which clearly demonstrated that the interaction between Fen1 and WT PCNA was much more resistant to high salt concentrations than the interaction between Fen1 and PCNA p.Ser228Ile (Figure 4C). This led us to conclude that in the SILAC experiments (Figure 4B), Fen1 remained bound to the WT PCNA column during the elution with 500 mM NaCl, resulting in a dramatic reduction of this protein in the WT eluate. Our conclusion that the p.Ser228Ile change impairs the ability of PCNA to bind Fen1 was further validated by subsequent immunoprecipitation and GST pulldown experiments (see below).

We assessed the effects of the PCNA p.Ser228Ile alteration in a more physiological setting by immunoprecipitation from lymphoblastoid cell extracts. While an interaction between Fen1 and PCNA was clearly demonstrated in controls, an intermediate level of interaction was detected in heterozygote cell lines, and the interaction was barely detectable in cells homozygous for PCNA p.Ser228Ile (Figure 4D). These data provided unambiguous confirmation that interaction of Fen1 with PCNA is dramatically reduced by the p.Ser228Ile mutation.

We have been unable to identify a commercially available antibody against Lig1 that is effective for immunoprecipitation from our lymphoblastoid extracts. Thus, in order to further investigate the effect of the PCNA p.Ser228Ile alteration on the interaction between PCNA and Lig1, we used an in vitro approach (16). Lysates

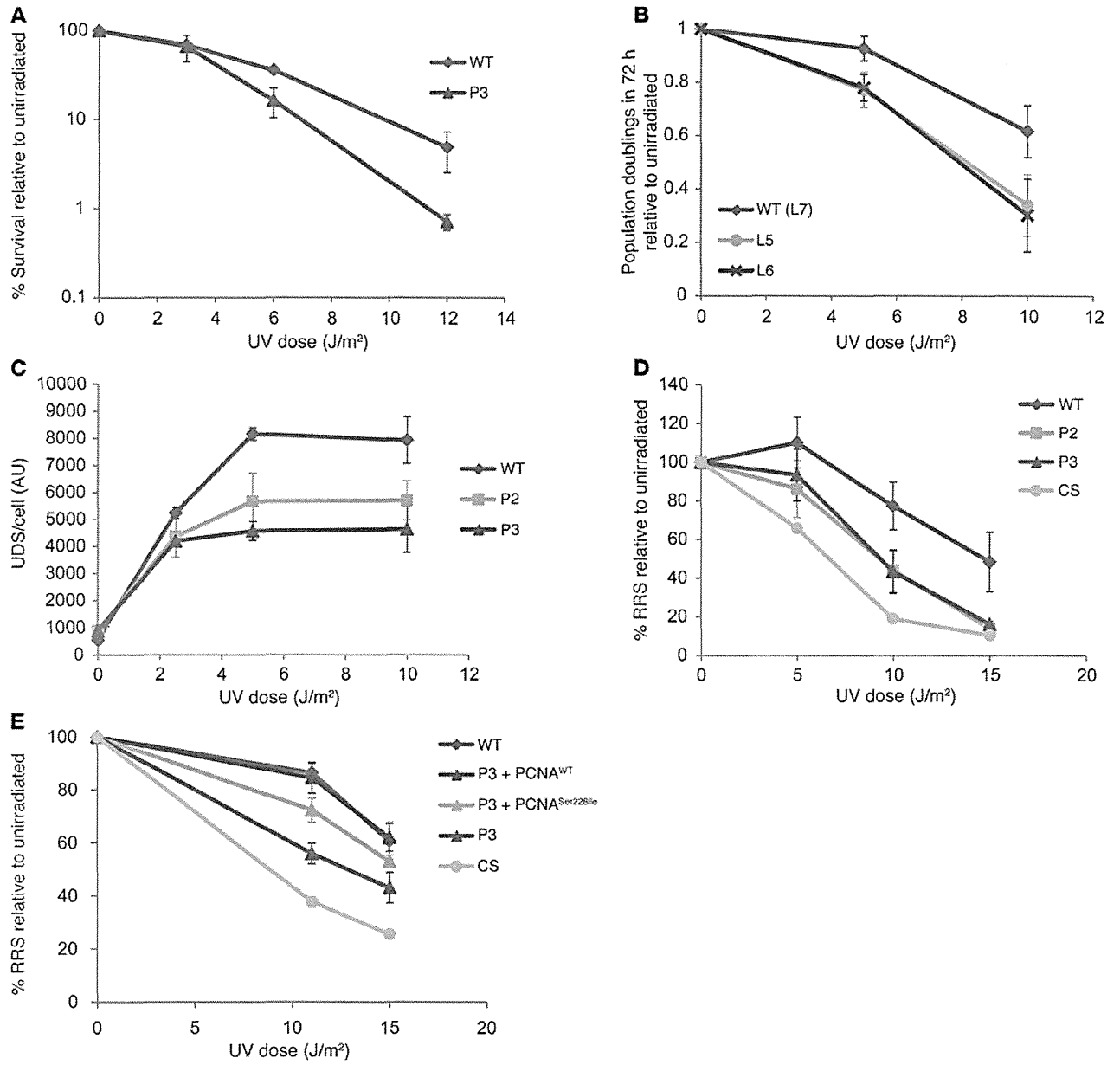

Figure 3

Abnormal cellular responses to UV. (**A**) Primary fibroblasts from an affected individual were sensitive to UV. Cell survival was measured by colony-forming ability after exposure to the indicated doses of UVC. (**B**) Lymphoblastoid cells from 2 different affected individuals were sensitive to UV. Viable cells were counted 72 hours after exposure to UVC using trypan blue exclusion. (**C**) Cells from affected individuals had reduced UDS activity. UDS was measured by incorporation of radiolabeled thymidine immediately after UV irradiation of nondividing cells with the indicated doses of UVC. (**D**) RRS, measured by incorporation of radiolabeled uridine 24 hours after UVC irradiation of nondividing cells with the indicated doses. A typical response of cells from a CS patient is shown for reference. (**E**) Defective RRS was complemented by lentiviral transduction of primary patient fibroblasts with WT PCNA. RRS was measured using EdU incorporation and automated high content microscopy in cells expressing high levels of ectopic PCNA. Values are mean and range of 2 experiments (**A**) or mean ± SEM of 3 (**B–D**) or 4 (**E**) experiments.

were prepared from *E. coli* expressing a fusion protein consisting of GST and the PIP box motif of either Fen1 or Lig1. These were then mixed with lysate containing PCNA (WT or p.Ser228Ile), glutathione beads were added, and the proteins associated with the beads were analyzed by SDS-PAGE. This assay recapitulated the defective interaction between PCNA p.Ser228Ile and Fen1 and, most significantly, showed that PCNA p.Ser228Ile also had a reduced affinity for the PIP box of Lig1 (Figure 4, E and F).

Given that Fen1 and Lig1 are both implicated in the NER pathways (17, 18), it is plausible that the cellular NER defects observed in cells from affected individuals result from the compromised interactions of these proteins with PCNA p.Ser288Ile. It also

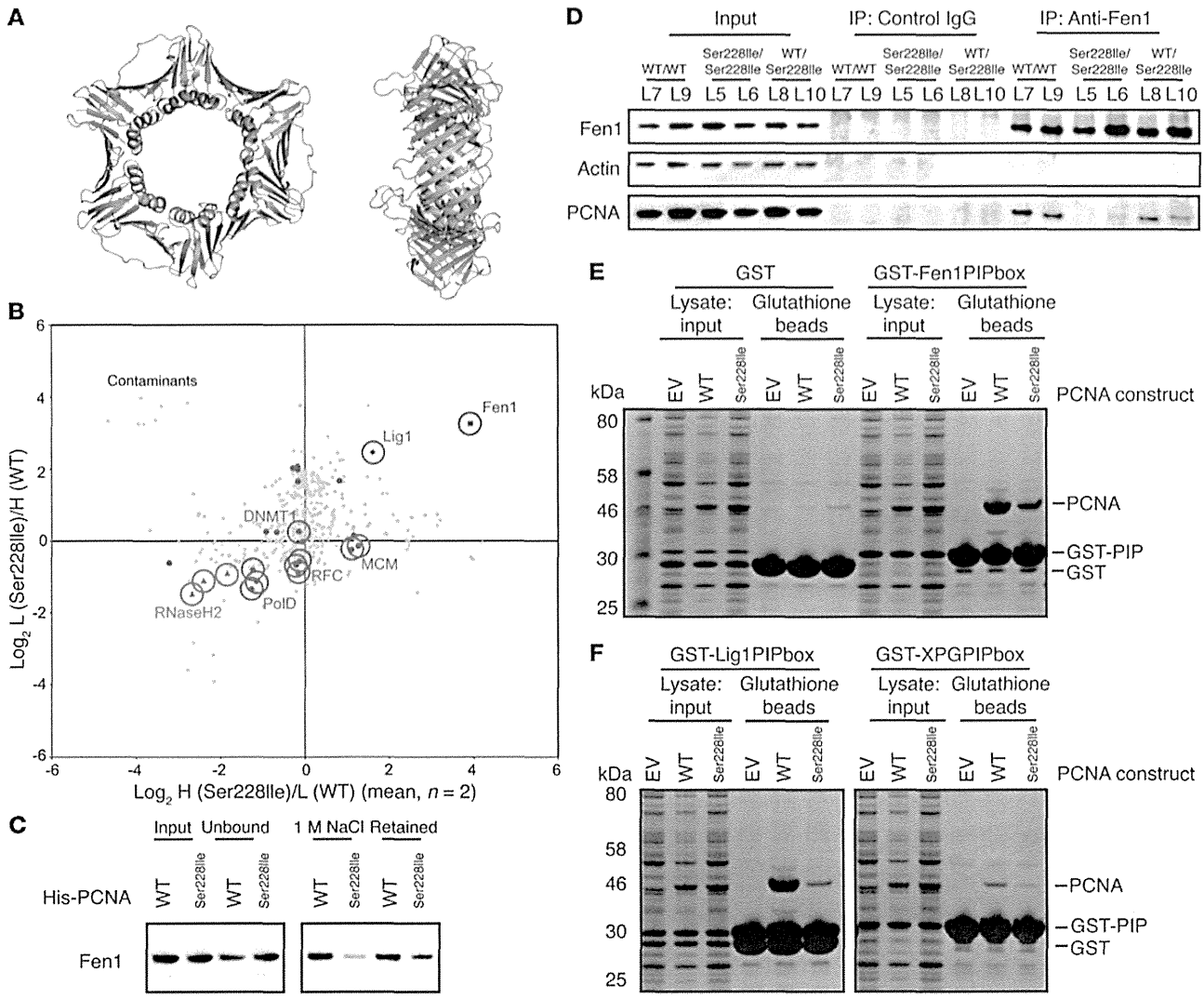

Figure 4

Perturbed PCNA interactions resulting from the p.Ser228Ile mutation. (**A**) Front and side views of the PCNA homotrimer, with Ser228 highlighted in magenta and the IDCL highlighted in cyan. Image was generated using POLYVIEW-3D (40), based on the 1YM crystal structure, rendered using PyMol. (**B**) Graphical representation of SILAC-based comparative PCNA-interaction analyses. Lysine [$^{13}C_6/^{15}N_2$] and arginine [$^{13}C_6/^{15}N_4$] labeled ("heavy"; H) or unlabeled ("light"; L) cell extracts were purified on PCNA WT or p.Ser228Ile affinity columns, and eluted proteins were analyzed by mass spectrometry. Each point represents the observed heavy/light ratios of a protein present in 3 of 3 experiments. Known PCNA-interacting proteins are shown in blue (see Supplemental Table 1). Proteins of particular interest are identified by name. (**C**) Recombinant His-PCNA (WT or p.Ser228Ile) was added to HeLa cell extracts and proteins bound to Ni-NTA. Proteins eluted at 1M NaCl or retained on the beads were analyzed by Western blot for Fen1. (**D**) Anti-Fen1 immunoprecipitates, from extracts made from lymphoblastoid lines derived from affected individuals or family members, were analyzed by Western blot for the presence of PCNA, Fen1, and actin. PCNA was almost undetectable in the precipitation from cell extracts derived from affected individuals. (**E**) *E. coli* lysates expressing empty vector (EV) or PCNA (WT or p.Ser228Ile) were mixed with lysates expressing GST or GST fused to the PIP box of Fen1. Inputs and glutathione-purified proteins were analyzed by SDS-PAGE and Coomassie staining. (**F**) Similar to **E**, except GST fusions comprising the PIP box of Lig1 and XPG were used.

seemed likely that the p.Ser228Ile alteration would perturb the PCNA interaction with other PIP box–containing partners and that this may contribute to the cellular phenotypes observed. One clear candidate, which is known to be required for NER and also to bind PCNA through a PIP box interaction, is XPG (16). We did not detect peptides derived from XPG in our SILAC assay, which by its nature will only detect relatively abundant proteins and relatively strong interactions. In the absence of an XPG antibody suitable for immunoprecipitation of endogenous XPG, the GST assay was again used to assess the binding of PCNA (WT and p.Ser228Ile) to the PIP box of XPG. Crucially, although less WT PCNA was bound to the XPG PIP box compared with its binding to the Fen1 PIP box, PCNA p.Ser228Ile displayed no detectable interaction with the XPG PIP box (Figure 4F). Thus, it seems reasonable to suggest that a defective interaction with XPG is also likely to contribute to the NER phenotype seen in cells homozygous for PCNA p.Ser228Ile.

Discussion

The genetic and cellular data described here implicated PCNA in a new, distinct neurodegenerative DNA repair disorder displaying some features in common with other conditions associated with deficient DNA metabolism, including CS, XP, and AT. The most notable similarities among CS, the neurological form of XP, and the individuals with the PCNA mutation described herein included growth abnormalities, premature aging, cognitive decline, photosensitivity, and photophobia. The presence of a basal cell carcinoma in situ in 1 affected individual (patient VI:11) likely indicates a predisposition to sun-induced malignancy in individuals homozygous for PCNA p.Ser228Ile and further clinical overlap with XP. However, the phenotype associated with PCNA p.Ser228Ile appears to be generally milder than that seen with typical CS or XP; most notably, the rate of premature aging seemed to be slower, with none of the ophthalmic manifestations associated with CS reported, and the effects of UV sensitivity appeared less substantial. Interestingly, although hearing loss is found in CS and some XP patients, the age of onset is typically later (1, 4). Thus, prelingual sensorineural hearing loss may, in association with the other clinical features described, be a helpful diagnostic feature in patients with this condition. The ocular and cutaneous telangiectasia seen in patients with the PCNA p.Ser228Ile mutation are reminiscent of those seen in AT, as was the pattern and progression of neurological abnormalities, although as with CS and XP, PCNA p.Ser228Ile homozygotes generally appeared to be less severely affected than typical AT patients. As with CS and XP, there were also striking differences between the phenotype associated with PCNA p.Ser228Ile and AT, including an absence of both the immunodeficiency and oculomotor apraxia commonly seen in AT-affected individuals.

Complete disruption of PCNA in flies or yeast is lethal (19, 20), an expected finding given its fundamental involvement in DNA replication. Until now, no pathological mutations in *PCNA* have been reported in human populations. In other species, however, some mutations of *PCNA* are compatible with life. For example, point mutations have been produced in *POL30* (encoding *S. cerevisiae* PCNA) that result in a wide variety of phenotypes, including DNA damage sensitivity, alterations in mutation rate, and epigenetic silencing defects (21). Similar phenotypes are seen in the various reported mutations in *mus209* (encoding *Drosophila* PCNA) (19). The only previously reported pathological mutation of *PCNA* in mammalian systems is a targeted missense mutation of lysine 164 to arginine (p.Lys164Arg) in mice, which was generated to assess the role of ubiquitination at this residue in somatic hypermutation in the immune system (9). Ubiquitination of PCNA at Lys164 is essential for translesion synthesis, a DNA damage tolerance process (22). Mice homozygous for *Pcna* p.Lys164Arg are viable but infertile and have an altered mutation spectrum of hypermutated Ig genes (9, 23). Thus, a subtle mutation of *PCNA* that impinges on a specific function can lead to characteristic loss-of-function effects on DNA metabolism.

Consistent with this, our present assays suggested that the PCNA p.Ser228Ile mutation described here is hypomorphic in nature. We did not detect any gross abnormalities of DNA replication associated with this mutation. Instead, we showed that the mutation had distinctive consequences for the cellular responses to UV, affecting both GG-NER and TC-NER. The effects on RRS seen in CS cell lines and on UDS in XP cell lines were typically more dramatic than we observed in homozygous PCNA p.Ser228Ile cells. This may explain, at least in part, why the phenotypic manifestations associated with these cellular abnormalities were not as profound in the individuals described herein compared with those seen in CS and XP.

Our findings defined particular defective interactions of PCNA p.Ser228Ile that are likely to be at least partly responsible for the specific alterations in cellular activities we observed, possibly together with other interactions not yet recognized. The altered protein interaction capability of PCNA p.Ser228Ile is also likely to account for the clinical manifestations of this syndrome. Complete abrogation of the PCNA-Fen1 interaction, mediated by a homozygous mutation of the Fen1 PIP box, is lethal in mice (24). Hence, it seems likely that while the p.Ser228Ile alteration dramatically reduces the association between PCNA and Fen1 in cell extracts, it is unlikely to completely abrogate their functional partnership. Consistent with this, our SILAC and interaction assays using recombinant proteins both showed that PCNA p.Ser228Ile remained capable of interacting with Fen1, although with markedly altered affinity. We cannot conclude from our assays whether the defective interactions with XPG, Fen1, and Lig1 are solely responsible for the observed effects on NER, although it is important to note that all these proteins are reported to be involved in this repair pathway (6, 17, 18). Thus, the perturbation of their interactions with PCNA could well be a major contributor to this abnormal cellular phenotype.

Mutations in XPG are rare and can be divided into 2 categories: missense mutations in the nuclease domains abrogate NER, but result in relatively mild XP phenotypes, whereas truncating mutations cause a very severe XP/CS complex disorder (25, 26). The *xpg*$^{-/-}$ mouse is barely viable (27). These varying phenotypes are thought to result because, in addition to its function in NER, XPG is involved in other processes (26). In particular, it associates with the transcription factor TFIIH and RNA polymerase II and has a role in transcription (25, 28, 29). The disruption of these other functions of XPG is suspected to be responsible for the more severe features of truncation mutations. For example, previously described patient XPCS1RO (94RD27) had severe early-onset CS and died at 7 months of age. He was homozygous for a frameshift mutation at codon 926 of *XPG*. This mutation leaves the nuclease domains intact, but truncates the protein before the PIP box and nuclear localization signal (30). Thus, the C-terminal region of XPG, including the motif responsible for interacting with PCNA, is very important for XPG function. These observations lead us to suggest that perturbation of PCNA's interaction with XPG may contribute to the neurological features associated with PCNA p.Ser228Ile.

In contrast to the homozygous state, mice heterozygous for the Fen1 PIP box mutant are viable, although they show predisposition to malignancy (31). Although specific PIP box mutations of Lig1 have not been generated in mammals, loss-of-function mutations in *LIG1* have been reported in a single individual, resulting in a complex human phenotype consisting of growth restriction, immunodeficiency, and photosensitivity (32), features reminiscent of those seen in PCNA p.Ser228Ile homozygotes. It is possible that Lig1 deficiency and PCNA p.Ser228Ile homozygosity together represent a group of conditions caused by disruption of multiple different DNA repair pathways. In addition, while the observed cellular defects correlated with the CS- and XP-like features of the syndrome, the clinical overlap with AT will require further investigation.

As well as being crucial to the maintenance of genomic integrity and prevention of neoplastic changes, DNA repair is known to be fundamentally important both during the rapid proliferative phase

characteristic of early neurogenesis and in the prevention of early cell death. The affected individuals with the PCNA mutation described herein displayed signs of neurodegeneration, a recognized feature of CS, AT, and neurological forms of XP, although the pathological patterns seen in each are distinct. More detailed investigation of the altered biological processes resulting from the PCNA p.Ser228Ile alteration should provide invaluable insight into the biological basis of this novel human disorder, as well as the neurodegenerative disease mechanisms involved in DNA damage tolerance and repair disorders. Further, although mutations resulting in complete loss of function of PCNA in humans may be incompatible with life, it remains an intriguing possibility that additional sequence variants in this gene, affecting other distinct aspects of PCNA function, might be viable and result in a phenotype more — or, indeed, less — severe than that associated with the p.Ser228Ile alteration described here.

Methods

Genetic studies. SNP genotyping was carried out using Illumina Human CytoSNP-12v2.1 330K arrays. Multipoint linkage analysis was performed with MERLIN (33) under a model of autosomal-recessive inheritance with full penetrance, assuming a disease allele frequency of 0.0001. Unique primers for sequencing and microsatellite analysis (Sigma-Aldrich) were designed using online software Primer3web (34) using sequences from the UCSC Genome Browser. RT-PCR was carried out using Clontech One Step RT-PCR Kit following the manufacturer's instructions, and bidirectional dideoxy DNA sequencing was performed on an ABI3130 XLA capillary sequencer (Applied Biosystems) with analysis using Finch TV 1.4.0 (Geospiza Inc.) and Gene Tool 1.0.0.1 (Bio Tools Inc.). Whole exome sequencing was performed by Otogenetics Corp. using the SureSelect Human All Exon V4 (Agilent Technologies) exome enrichment kit on an Illumina HiSeq2000. The exome sequencing produced 31,783,299 mapped reads, corresponding to 93% of targeted sequences covered sufficiently for variant calling (> 10× coverage; mean depth, 45×).

Cell studies. Cells were cultured in DMEM/RPMI (Sigma Aldrich) with 15% FBS (FCS-Hyclone), 2 mM glutamine (Invitrogen), and 1% penicillin and streptomycin. UV sensitivity of lymphoblastoid cells was determined by irradiating cells in PBS (1×10^6 viable cells in 1 ml) with UVC (254 nm, 1 $Jm^{-2}s^{-1}$), adding 4 ml growth medium and counting viable cells using trypan blue exclusion after a 72-hour recovery period. UDS, RNA synthesis, fibroblast survival assays, and lentivirus-mediated complementation were performed as described previously (10–12, 35–37).

Protein interaction analyses. Recombinant PCNA WT and PCNA p.Ser228Ile were produced with a His-tag from pET28b in *E. coli* BL21 codonplus (Novagen) and purified on Ni-NTA sepharose (QIAGEN). Affinity columns were made by covalently linking these proteins to NHS-activated sepharose (Pierce). For SILAC analysis, HeLa cells were grown in SILAC DMEM (Gibco) supplemented with 10% dialyzed FBS, 2 mM $CaCl_2$, 1 mM $MgSO_4$, 52 mg/l L-leucine, and 100 mg/l L-lysine and L-arginine (for "heavy" extracts, we substituted [$^{13}C_6/^{15}N_2$] lysine and [$^{13}C_6/^{15}N_4$] arginine; CKgas). Extracts were made by lysing cells in a low-salt buffer containing benzonase (Merck), then adjusting to 150 mM NaCl. All protein interaction assays were performed in interaction buffer (25 mM Tris pH 7.5, 25 mm NaCl, 10% glycerol, 0.01% Igepal, 1 mM PMSF). Proteins eluted from PCNA affinity columns with 500 mM NaCl were combined before 10-fraction mass spectrometric (MS-MS) analysis (MS Bioworks). Data were analyzed, and H/L ratios were determined using MaxQuant software. To further analyze the stability of PCNA interactions, recombinant PCNAs were added to HeLa nuclear extract (4C), and complexes were isolated on Ni-NTA agarose and sequentially washed and eluted with increasing [NaCl]. For immunoprecipitation, protein extracts were made from lymphoblastoid cells as described above. Fen1 protein was precipitated using an anti-Fen1 rabbit antibody (EPR4459[2]; GeneTex) and protein A/G dynabeads (Invitrogen). Proteins in the extracts and precipitates were analyzed by Western blot with anti-PCNA (PC10; Abcam) or anti-Fen1 (4E7; GeneTex). GST fusion protein association studies were performed as previously described (16), using lysates from *E. coli* harboring pET30a as a control, or PCNA (WT or p.Ser228Ile) expressed from pET30a. These were mixed, in a buffer containing 100 mM KH_2PO_4/K_2HPO_4, with lysates from *E. coli* expressing glutathione S transferase (GST) or fusion proteins comprising GST and the PIP boxes of Fen1 (aa 328–355), XPG (aa 981–1,009), or Lig1 (aa 1–21 with an 8-aa glycine-serine spacer to maintain equal distance between the GST and the PIP box in all cases).

Western blotting. Exponentially growing primary human fibroblast cells were lysed on ice in 50 mM Tris-HCl pH 7.5, 150 mM NaCl, 200 μM EDTA, and 1% NP-40. Extracts were clarified by centrifugation at 10,000 *g* for 10 minutes at 4°C, then fractionated by SDS-PAGE. Proteins were transferred to Protran nitrocellulose (Whatman) and immunoblotted with anti-PCNA (PC10; Abcam) or anti-Fen1 (4E7; GeneTex). ATM kinase activity assay and Western blotting of ATM and associated proteins in lymphoblastoid cells was carried out as described previously (38).

FACS analysis of cell cycle position. Primary fibroblasts were incubated with 10 μM BrdU for 30 minutes, then trypsinized and fixed by addition of methanol to 70%. After storage at –20°C, cells were treated with 0.2 mg/ml pepsin in 2M HCl for 20 minutes, then incubated in 0.5% BSA in PBS with 0.5% Tween 20 and anti-BrdU antibody (1:50 dilution; BD) for 1 hour. Cells were then subjected to washing in 0.5% BSA and incubation with 1:100 anti-mouse secondary antibody coupled to Alexa Fluor 488 (Molecular Probes) for 30 minutes, followed by washing and resuspension in PBS with 0.5 mg/ml RNaseA for 15 minutes. Propidium iodide (10 μg/ml) was added just before analysis on a CyAn ADP Analyzer (Beckman Coulter Inc.).

Immunofluorescence. 5-ethynyl-2′-deoxyuridine (EdU) staining was carried out using the Click-iT EdU Alexa Fluor 555 Imaging Kit (Invitrogen). Cells were seeded onto glass coverslips so as to be subconfluent at the time of fixation. At least 24 hours after plating, EdU was added to the culture medium to a final concentration of 20 μM, and cells were returned to 37°C for 10 minutes. Soluble proteins were extracted by rinsing once in PBS and once in CSK buffer (100 mM NaCl, 300 mM sucrose, 10 mM PIPES pH 7.0, and 3 mM $MgCl_2$), then soaking in CSK plus 0.2% Triton X-100 for 5 minutes on ice. After a further wash in CSK, cells were fixed (ice-cold methanol for 20 minutes at –20°C), washed twice more in PBS, and then blocked (5% w/v BSA in PBST) for 30 minutes at room temperature. EdU staining was carried out according to the manufacturer's instructions. Coverslips were then incubated for 1 hour at room temperature in blocking buffer containing anti-PCNA monoclonal antibody (PC-10) diluted 1:1,000, followed by 3 washes in PBST and incubation in Alexa Fluor 488 goat anti-rabbit IgG (Invitrogen) diluted 1:1,000 in blocking buffer for 45 minutes. Cells were rinsed a further 3 times in PBST, and coverslips were mounted in Aqua-Poly/Mount (Polysciences) containing DAPI at a final concentration of 1.5 μg/ml. Slides were visualized using a Leica SP5 confocal microscope.

DNA fiber analysis. Immunolabeling of DNA fiber spreads was carried out as described previously (39), with minor modifications. Cells were incubated in 5-iodo-2′-deoxyuridine (IdU) and 5-chloro-2′-deoxyuridine (CldU) at a final concentration of 100 μM for 20 minutes each, and all antibody incubations were for 2 hours at room temperature. Fibers were mounted in ProLong mounting medium (Invitrogen).

Statistics. In graphical representations of experimental data, error bars represent SEM or range of the plotted mean of at least 2 independent experiments, as indicated in the figure legends.

Study approval. The present studies in humans were reviewed and approved (reference 10-0050-01) by the Institutional Review Board of the Office for the Responsible Conduct of Research, University of Arizona (Tucson, Arizona, USA). All tissue samples were taken with informed con-

sent in accordance with all ethical standards and protocols. Subjects or their guardians provided informed consent prior to their participation in the study. Written informed consent was obtained to publish the photographs of affected individuals.

Acknowledgments

We are grateful to the families for partaking in this study and to the Amish community for their continuing support of the Windows of Hope project. We are grateful to Luther Robinson for contributing clinical data, Kristiana Gordon for review of the dermatology, Wendy Albuquerque for review of the audiograms, and Jon Wing for technical assistance. Chromosome breakage studies were carried out at GSTS Pathology, and karyotyping was performed at South West Thames Genetics Laboratory. Illumina cytoSNP analysis and Sanger sequencing were carried out at the Medical Biomics Centre, St. George's University of London. FACS analysis was done by Drew Worth in the Flow Cytometry Core Facility of the Jenner Institute, Oxford. The work was supported by MRC Clinical Research Training fellowship G1001931 (to E.L. Baple), MRC grant G1002279 (to A.H. Crosby), MRC centenary fund award G0900205 (St. George's University of London, E.L. Baple), the Newlife Foundation for disabled children (to E.L. Baple and A.H. Crosby), Cancer Research UK career development fellowship C24125/A8307 (to C.M. Green), and Wellcome Trust Core Award 090532/Z/09/Z (to C.M. Green).

Received for publication December 4, 2013, and accepted in revised form April 17, 2014.

Address correspondence to: Andrew H. Crosby, Medical Research (Level 4), RILD Wellcome Wolfson Centre, Royal Devon and Exeter NHS Foundation Trust, Barrack Road, Exeter EX2 5DW, United Kingdom. Phone: 1392.408302; Fax: 1392.408388; E-mail: A.H.Crosby@exeter.ac.uk. Or to: Catherine M. Green, Wellcome Trust Centre for Human Genetics, University of Oxford, Roosevelt Drive, Oxford OX3 7BN, United Kingdom. Phone: 1865.287510; Fax: 1865.287501; E-mail: catherine.green@well.ox.ac.uk.

1. DiGiovanna JJ, Kraemer KH. Shining a light on xeroderma pigmentosum. *J Invest Dermatol.* 2012; 132(3 Pt 2):785–796.
2. Perlman S, Becker-Catania S, Gatti RA. Ataxia-telangiectasia: diagnosis and treatment. *Semin Pediatr Neurol.* 2003;10(3):173–182.
3. Kamileri I, Karakasilioti I, Garinis GA. Nucleotide excision repair: new tricks with old bricks. *Trends Genet.* 2012;28(11):566–573.
4. Nance MA, Berry SA. Cockayne syndrome: review of 140 cases. *Am J Med Genet.* 1992;42(1):68–84.
5. Cleaver JE. Photosensitivity syndrome brings to light a new transcription-coupled DNA repair cofactor. *Nat Genet.* 2012;44(5):477–478.
6. Cleaver JE, Lam ET, Revet I. Disorders of nucleotide excision repair: the genetic and molecular basis of heterogeneity. *Nat Rev Genet.* 2009;10(11):756–768.
7. Shivji KK, Kenny MK, Wood RD. Proliferating cell nuclear antigen is required for DNA excision repair. *Cell.* 1992;69(2):367–374.
8. Moldovan GL, Pfander B, Jentsch S. PCNA, the maestro of the replication fork. *Cell.* 2007; 129(4):665–679.
9. Langerak P, Nygren AO, Krijger PH, van den Berk PC, Jacobs H. A/T mutagenesis in hypermutated immunoglobulin genes strongly depends on PCNAK164 modification. *J Exp Med.* 2007; 204(8):1989–1998.
10. Lehmann AR, Stevens S. A rapid procedure for measurement of DNA repair in human fibroblasts and for complementation analysis of xeroderma pigmentosum cells. *Mutat Res.* 1980;69(1):177–190.
11. Mayne LV, Lehmann AR. Failure of RNA synthesis to recover after UV irradiation: an early defect in cells from individuals with Cockayne's syndrome and xeroderma pigmentosum. *Cancer Res.* 1982; 42(4):1473–1478.
12. Nakazawa Y, et al. Mutations in UVSSA cause UV-sensitive syndrome and impair RNA polymerase IIo processing in transcription-coupled nucleotide-excision repair. *Nat Genet.* 2012;44(5):586–592.
13. Gulbis JM, Kelman Z, Hurwitz J, O'Donnell M, Kuriyan J. Structure of the C-terminal region of p21(WAF1/CIP1) complexed with human PCNA. *Cell.* 1996;87(2):297–306.
14. Warbrick E. PCNA binding through a conserved motif. *Bioessays.* 1998;20(3):195–199.
15. Bruning JB, Shamoo Y. Structural and thermodynamic analysis of human PCNA with peptides derived from DNA polymerase-delta p66 subunit and flap endonuclease-1. *Structure.* 2004; 12(12):2209–2219.
16. Gary R, Ludwig DL, Cornelius HL, MacInnes MA, Park MS. The DNA repair endonuclease XPG binds to proliferating cell nuclear antigen (PCNA) and shares sequence elements with the PCNA-binding regions of FEN-1 and cyclin-dependent kinase inhibitor p21. *J Biol Chem.* 1997; 272(39):24522–24529.
17. Araujo SJ, et al. Nucleotide excision repair of DNA with recombinant human proteins: definition of the minimal set of factors, active forms of TFIIH, and modulation by CAK. *Genes Dev.* 2000; 14(3):349–359.
18. Wu Z, et al. High risk of benzo[alpha]pyrene-induced lung cancer in E160D FEN1 mutant mice. *Mutat Res.* 2012;731(1–2):85–91.
19. Henderson DS, Banga SS, Grigliatti TA, Boyd JB. Mutagen sensitivity and suppression of position-effect variegation result from mutations in mus209, the Drosophila gene encoding PCNA. *EMBO J.* 1994;13(6):1450–1459.
20. Waseem NH, Labib K, Nurse P, Lane DP. Isolation and analysis of the fission yeast gene encoding polymerase delta accessory protein PCNA. *EMBO J.* 1992;11(13):5111–5120.
21. Zhang Z, Shibahara K, Stillman B. PCNA connects DNA replication to epigenetic inheritance in yeast. *Nature.* 2000;408(6809):221–225.
22. Kannouche PL, Wing J, Lehmann AR. Interaction of human DNA polymerase eta with monoubiquitinated PCNA: a possible mechanism for the polymerase switch in response to DNA damage. *Mol Cell.* 2004;14(4):491–500.
23. Langerak P, Krijger PH, Heideman MR, van den Berk PC, Jacobs H. Somatic hypermutation of immunoglobulin genes: lessons from proliferating cell nuclear antigenK164R mutant mice. *Philos Trans R Soc Lond B Biol Sci.* 2009;364(1517):621–629.
24. Zheng L, Dai H, Qiu J, Huang Q, Shen B. Disruption of the FEN-1/PCNA interaction results in DNA replication defects, pulmonary hypoplasia, pancytopenia, and newborn lethality in mice. *Mol Cell Biol.* 2007;27(8):3176–3186.
25. Clarkson SG. The XPG story. *Biochimie.* 2003; 85(11):1113–1121.
26. Scharer OD. XPG: its products and biological roles. *Adv Exp Med Biol.* 2008;637:83–92.
27. Harada YN, et al. Postnatal growth failure, short life span, and early onset of cellular senescence and subsequent immortalization in mice lacking the xeroderma pigmentosum group G gene. *Mol Cell Biol.* 1999;19(3):2366–2372.
28. Sarker AH, et al. Recognition of RNA polymerase II and transcription bubbles by XPG, CSB, and TFIIH: insights for transcription-coupled repair and Cockayne Syndrome. *Mol Cell.* 2005;20(2):187–198.
29. Ito S, et al. XPG stabilizes TFIIH, allowing transactivation of nuclear receptors: implications for Cockayne syndrome in XP-G/CS patients. *Mol Cell.* 2007; 26(2):231–243.
30. Nouspikel T, Lalle P, Leadon SA, Cooper PK, Clarkson SG. A common mutational pattern in Cockayne syndrome patients from xeroderma pigmentosum group G: implications for a second XPG function. *Proc Natl Acad Sci U S A.* 1997;94(7):3116–3121.
31. Zheng L, et al. Fen1 mutations that specifically disrupt its interaction with PCNA cause aneuploidy-associated cancer. *Cell Res.* 2011;21(7):1052–1067.
32. Barnes DE, Tomkinson AE, Lehmann AR, Webster AD, Lindahl T. Mutations in the DNA ligase I gene of an individual with immunodeficiencies and cellular hypersensitivity to DNA-damaging agents. *Cell.* 1992;69(3):495–503.
33. Abecasis GR, Wigginton JE. Handling marker-marker linkage disequilibrium: pedigree analysis with clustered markers. *Am J Hum Genet.* 2005; 77(5):754–767.
34. Rozen S, Skaletsky H. Primer3 on the WWW for general users and for biologist programmers. *Methods Mol Biol.* 2000;132:365–386.
35. Lehmann AR, Thompson AF, Harcourt SA, Stefanini M, Norris PG. Cockayne's syndrome: correlation of clinical features with cellular sensitivity of RNA synthesis to UV irradiation. *J Med Genet.* 1993; 30(8):679–682.
36. Arlett CF, Harcourt SA, Cole J, Green MH, Anstey AV. A comparison of the response of unstimulated and stimulated T-lymphocytes and fibroblasts from normal, xeroderma pigmentosum and trichothiodystrophy donors to the lethal action of UV-C. *Mutat Res.* 1992;273(2):127–135.
37. Nakazawa Y, Yamashita S, Lehmann AR, Ogi T. A semi-automated non-radioactive system for measuring recovery of RNA synthesis and unscheduled DNA synthesis using ethynyluracil derivatives. *DNA Repair (Amst).* 2010;9(5):506–516.
38. Reiman A, et al. Lymphoid tumours and breast cancer in ataxia telangiectasia; substantial protective effect of residual ATM kinase activity against childhood tumours. *Br J Cancer.* 2011;105(4):586–591.
39. Unsal-Kacmaz K, et al. The human Tim/Tipin complex coordinates an Intra-S checkpoint response to UV that slows replication fork displacement. *Mol Cell Biol.* 2007;27(8):3131–3142.
40. Porollo A, Meller J. Versatile annotation and publication quality visualization of protein complexes using POLYVIEW-3D. *BMC Bioinformatics.* 2007;8:316.

Dadras SS (2011) Molecular diagnostics in melanoma: current status and perspectives. *Arch Pathol Lab Med* 135:860–9

Damjanov I, Katic V, Stevens LC (1975) Ultrastructure of ovarian teratomas in LT mice. *Z Krebsforsch Klin Onkol Cancer Res Clin Oncol* 83:261–7

Damsky WE Jr., Bosenberg M (2010) Mouse melanoma models and cell lines. *Pigment Cell Melanoma Res* 23:853–9

Fidler IJ (1975) Biological behavior of malignant melanoma cells correlated to their survival *in vivo*. *Cancer Res* 35:218–24

Krupke DM, Begley DA, Sundberg JP *et al.* (2008) The Mouse Tumor Biology Database. *Nat Rev Cancer* 8:459–65

Lee GH, Bugni JM, Obata M *et al.* (1997) Genetic dissection of susceptibility to murine ovarian teratomas that originate from parthenogenetic oocytes. *Cancer Res* 57:590–3

Maronpot R, Boorman GA, Gaul BW (1999) *Pathology of the Mouse, Reference and Atlas* Vienna: Cache River Press

Naf D, Krupke DM, Sundberg JP *et al.* (2002) The Mouse Tumor Biology Database: a public resource for cancer genetics and pathology of the mouse. *Cancer Res* 62:1235–40

Schofield PN, Gruenberger M, Sundberg JP (2010) Pathbase and the MPATH ontology. Community resources for mouse histopathology. *Vet Pathol* 47:1016–20

Silva K, Sundberg JP (2012) Necropsy methods. In: *The Laboratory Mouse* Hedrich H (ed) 2nd edn London: Academic Press, 779–806

Sundberg JP, Sundberg BA, Beamer WG (1997) Comparison of chemical carcinogen skin tumor induction efficacy in inbred, mutant, and hybrid strains of mice: morphologic variations of induced tumors and absence of a papillomavirus cocarcinogen. *Mol Carcinog* 20:19–32

Walker GJ, Soyer HP, Terzian T *et al.* (2011) Modelling melanoma in mice. *Pigment Cell Melanoma Res* 24:1158–76

Zembowicz A, Carney JA, Mihm MC (2004) Pigmented epithelioid melanocytoma: a low-grade melanocytic tumor with metastatic potential indistinguishable from animal-type melanoma and epithelioid blue nevus. *Am J Surg Pathol* 28:31–40

Zembowicz A, Knoepp SM, Bei T *et al.* (2007) Loss of expression of protein kinase a regulatory subunit 1alpha in pigmented epithelioid melanocytoma but not in melanoma or other melanocytic lesions. *Am J Surg Pathol* 31:1764–75

Differences in Clinical Phenotype among Patients with XP Complementation Group D: 3D Structure and ATP-Docking of XPD *In Silico*

Journal of Investigative Dermatology (2014) **134,** 1775–1778; doi:10.1038/jid.2014.14; published online 13 February 2014

TO THE EDITOR

Xeroderma pigmentosum (XP) is an autosomal recessive hereditary disease that is classified into seven genetic complementation groups, A through G, of nucleotide excision repair (NER)-deficient types and one NER-proficient variant type (DiGiovanna and Kraemer, 2012). Patients with XP complementation group D (XPD) display photosensitivity, proneness to skin cancer and neurological symptoms, but the severity varies. In XPD from Western countries, the single amino-acid change R683W is found in 73% of the patients and most of them suffer from neurological symptoms (Takayama *et al.*, 1995; Kobayashi *et al.*, 1997; Taylor *et al.*, 1997; Viprakasit *et al.*, 2001; Kobayashi *et al.*, 2002; Boyle *et al.*, 2008; Emmert *et al.*, 2009; Ueda *et al.*, 2009). In contrast, Japanese patients display only skin manifestations without neurological symptoms (Kobayashi *et al.*, 1997; Taylor *et al.*, 1997; Kobayashi *et al.*, 2002). XPD protein is an ATP-dependent 5′-3′ DNA helicase, which exerts unwinding of a damaged DNA strand to facilitate repair of the DNA. Although the human XPD protein remains refractory to crystallization, the crystal structure of XPD proteins from the archea has been solved (Fan *et al.*, 2008; Liu *et al.*, 2008). These structures revealed that XPD functions as a helicase with two helicase motifs separated by an ATP-binding cleft and two additional domains, a Fe–S cluster and an Arch domain.

In this study, we present six cases of Japanese XPD without neurological abnormalities in four families. All patients showed severe photosensitivity since birth, and their skin in the sun-exposed areas was hyperpigmented and covered with numerous pigmented maculae with color variations from light brown to dark brown. Four patients developed skin cancer, but none of them show neurological signs. XPD1KO and XPD4KO were assessed by a neurologist and an otorhinologist. Their clinical characteristics have been summarized in Table 1.

To determine the ability to repair UV-induced DNA damage, a colony-formation assay after UV irradiation and UV-induced unscheduled DNA synthesis (UDS) was assessed (Materials and Methods are described in Supplementary data). The dose range giving 37% cell survival and UV-induced UDS in patients' cells was much lower compared with that in the healthy subjects but was higher than that in XP-A cells (Table 1). Genetic complementation tests were carried out by means of a host-cell reactivation assay. Luciferase activity was increased specifically when *XPD* cDNA was cotransfected into each patient's cells. Therefore, we concluded that all cases belonged to XPD. Direct sequence analysis was performed on each exon of the genomic DNA of

Abbreviations: NER, nucleotide excision repair; UDS, unscheduled DNA synthesis; XP, xeroderma pigmentosum; XPD, xeroderma pigmentosum complementation group D

Accepted article preview online 13 January 2014; published online 13 February 2014

Table 1. Clinical and cellular characteristics of patients in the present study and the summary of reported cases with homozygous R683W and R683Q

								Mutations of *XPD* gene			
								Allele 1		Allele 2	
Case	Age/sex	Consanguinity	MED (mJ cm^{-2})	Skin cancer[3]	Neurological symptoms	UDS (%)	UV survival (D_{37};J m^{-2})	Genome	Amino acid	Genome	Amino acid
XPD1KO[1]	56/F	+	33	+(44)	–	27.3	1.5	c.2048A>G	p.R638Q	c.1855del3nt	p.del619
XPD2KO[1]	52/F	+	ND	+(38)	–	32	2.1	c.2048A>G	p.R638Q	c.1855del3nt	p.del619
XPD3KO	48/F	+	40	–	–	35.7	1.1	c.1621A>C	p.S541R	c.1621A>C	p.S541R
XPD4KO[2]	21/F	+	40	+(21)	–	26	1.25	c.2048A>G	p.R638Q	c.1102C>T	p.Q368X
XPD5KO[2]	19/M	+	60	–	–	30	2.1	c.2048A>G	p.R638Q	c.1102C>T	p.Q368X
XPD6KO	61/F	–	40	+(61)	–	ND	ND	c.1621A>C	p.S541R	c.1621A>C	p.S541R

Mutations of *XPD* gene	Number	Age (mean)	Skin cancer[4]	Neurological symptoms[4]	References
p.R638W	7	24.3	5/5(<15.4[5])	7/7	Taylor *et al.*, 1997; Viprakasit *et al.*, 2001
p.R638Q	7	34.1	4/5(35.3[6])	4/7	Taylor *et al.*, 1997; Falik-Zaccai *et al.*, 2012

Abbreviations: F, female; M, male; MED, minimal erythema dose; ND, not done; UDS, unscheduled DNA synthesis; XPD, xeroderma pigmentosum group D.
[1]XPD1KO and XPD2KO are siblings.
[2]XPD4KO and XPD5KO are siblings.
[3]The number indicates the age of onset of skin cancer.
[4]The number of cases who had symptoms of described cases.
[5]The age of onset of skin cancer was assumed to be younger than the age of patients with skin cancer.
[6]The average age at first diagnosis of skin cancer, which is described in 3 of 4 cases.

XPD in all patients. In XPD1KO and XPD2KO, one allele had a deletion of three nucleotides starting from nucleotide 1855, which causes an in-frame frameshift, causing a deletion of codon 619, and the other allele had a G-to-A substitution at nucleotide 2048. This single-base change causes R683Q. XPD3KO and XPD6KO showed a homozygous mutation of A-to-C at nucleotide 1261, which causes S541R. XPD4KO and XPD5KO were found to be compound heterozygotes of R683Q and Q368X, the latter being a nonsense mutation caused by a C-to-T change at nucleotide 1102.

To investigate the effects of these mutations, we obtained three dimensional (3D) structures of the wild-type XPD protein from ModBase (http://modbase.compbio.ucsf.edu/) and then constructed 3D structures of the mutant proteins (R683W, R683Q, S541R, and del619) *in silico*. These mutant proteins had alterations in the molecular conformation (Figure 1a) and in electrostatic surface potentials (Figure 1b) compared with the wild-type protein. The ATP-binding sites (Figure 1c) were positive-potential areas in the wild-type protein, whereas in mutant proteins they were negative-potential areas. In an ATP-docking simulation with each protein, we detected 50 instances of ATP docking out of 100 runs in wild-type protein, when the ATP direction was in the previously reported (natural or correct) orientation, whereas in the S541R, del619, and R683Q mutants, we detected 22, 32, and 34 instances, respectively. We did not detect ATP docking into the R683W mutant (Figure 1d). These data theoretically suggest that S541R, del619, and R683Q may be capable of interacting with ATP, although the binding is less stable compared with the wild-type, whereas R683W probably fails to interact with ATP.

To our knowledge, reports exist of 37 cases in whom authors have described both genetic analysis and the presence or absence of neurological symptoms. Combining these 37 cases with our 6 makes a total of 43 cases, and among them, there are 7 cases with homozygous R683W (Taylor *et al.*, 1997; Viprakasit *et al.*, 2001) and 7 cases with homozygous R683Q (Taylor *et al.*, 1997; Falik-Zaccai *et al.*, 2012). In patients with homozygous R683Q, three are free from neurological symptoms, three showed modest neurological symptoms and one was reported to display neurological symptoms. However, among patients with homozygous R683W, six displayed neurological symptoms and one showed ambiguous symptoms (Table 1). As for the skin symptoms, among cases with description of skin cancers, all patients with homozygous R683W developed skin cancer, as did four out of five with homozygous R683Q. The age of onset of skin tumor in homozygous R683Q was 20 years older than the average of the age in the cases with R683W (Table 1).

Most of the mutations in the *XPD* gene are located in the helicase domains, suggesting that these mutations reduce DNA binding and ATPase activity (Fan *et al.*, 2008). R683 is located in a conserved helicase motif and helicase activity of R683W has been reported to be lower than that in wild type (Ueda *et al.*, 2009) or none (Liu *et al.*, 2008). Comparison of R683W and R683Q with archaeal XPD shows that the latter mutation has more ATPase activity and single-strand DNA